95-83-7217
MOTC-IOT-94-H2DA003

訊號分析法比較研究暨其於水波應用探討 —
新型類仔波函數及其時尺轉換特性與應用

交 通 部 運 輸 研 究 所

中華民國 95 年 4 月

95-83-7217
MOTC-IOT-94-H2DA003

訊號分析法比較研究暨其於水波應用探討 —
新型類仔波函數及其時尺轉換特性與應用

著 者：李勇榮

交 通 部 運 輸 研 究 所
中華民國 95 年 4 月

新型類仔波函數及其時尺轉換特性與應用

著　　者：李勇榮
出版機關：交通部運輸研究所
地　　址：臺北市敦化北路 240 號
網　　址：www.ihmt.gov.tw (中文版＞中心出版品)
電　　話：(04) 26587176
出版年月：中華民國 95 年 4 月
印 刷 者：
版(刷)次冊數：初版一刷 110 冊
本書同時登載於交通部運輸研究所港灣技術研究中心網站
定　　價： 100 元
展 售 處：
交通部運輸研究所運輸資訊組•電話：(02)23496880
國家書坊臺視總店：臺北市八德路 3 段 10 號 B1•電話：(02)25781515
五南文化廣場：臺中市中山路 2 號 B1•電話：(04)22260330

GPN：1009500980　　　ISBN：986-00-4980-7(平裝)

95

新型類仔波函數及其時尺轉換特性與應用

交通部運輸研究所

GPN:1009500980
定價 100　元

交通部運輸研究所自行研究計畫出版品摘要表

出版品名稱：訊號分析法比較研究暨其於水波應用探討 —
新型類仔波函數及其時尺轉換特性與應用

國際標準書號（或叢刊號）	政府出版品統一編號	運輸研究所出版品編號	計畫編號
ISBN 986-00-4980-7 (平裝)	1009500980	95-83-7217	94-H2DA003

主辦單位：港灣技術研究中心
主管：邱永芳
計劃主持人：李勇榮
研究人員：李勇榮
聯絡電話：04-26587183
傳真號碼：04-26587183、 04-26571329

研究期間
自 94 年 01 月
至 94 年 12 月

關鍵詞：新型類仔波函基、模值與相位、時頻分析瞬間頻率、能脊線分佈、驗證與比較、頻漏現象、模糊效應、相位糙訊、比較於莫利仔波之優越性、側頻不穩現象、應用物理表徵。

摘要：

本文提出一新型類仔波複數函基函數，並說明其模值與相位之介定與數值求取方式。此類仔波於時頻分析瞬間頻率之擷取或能脊線分佈之檢測上具有較莫利仔波更為明確容易之優越性。此外，其模值與相位時尺分佈圖均可提供有義訊息。文中以各種模擬訊號及水槽試驗水波訊號來驗證與比較。另亦探討其表現之各項相關學理因子，如頻漏現象、模糊效應、相位糙訊、能脊規範等。也因為這些特性，其優異功能得加以解說，而其應用得以突顯一些物理表徵。

出版日期	頁數	定價	本 出 版 品 取 得 方 式
95 年 4 月	86	100	凡屬機密性出版品均不對外公開。普通性出版品，公營、公益機關團體及學校可函洽本所免費贈閱；私人及私營機關團體可按定價價購。

機密等級：
□密□機密 □極機密 □絕對機密
（解密條件：□ 年 月 日解密，□公布後解密，□附件抽存後解密，
□工作完成或會議終了時解密，□另行檢討後辦理解密）
■普通

備註：本研究之結論與建議不代表交通部之意見。

PUBLICATION ABSTRACTS OF RESEARCH PROJECTS
INSTITUTE OF TRANSPORTATION
MINISTRY OF TRANSPORTATION AND COMMUNICATIONS

TITLE: Time-Frequency Analyses and Their Applications – A Quasi Wavelet Basis Function for Improved Time-Frequency Characterizations

ISBN(OR ISSN)	GOVERNMENT PUBLICATIONS NUMBER	IOT SERIAL NUMBER	PROJECT NUMBER
ISBN 986-00-4980-7 (pbk)	1009500980	95-83-7217	94-H2DA003

DIVISION: HARBOR & MARINE TECHNOLOGY CENTER
DIVISION DIRECTOR: Yung-Fang Chiu
PRINCIPAL INVESTIGATOR: Yueon-Ron Lee
PROJECT STAFF: Yueon-Ron Lee
PHONE: 886-4-26587183
FAX: 886-4-26587183, 886-4-26571329

PROJECT PERIOD
FROM January 2005
TO December 2005

KEY WORDS: New Wavelet Variant Versus Morlet Wavelet, Time-Frequency Analyzing Kernel, Quasi Basis Function, Ridge Extractions, Modulus and Phase Planes, Frequency Leakages, Phase Noise and Ambiguity Effects, Side Band Instability

ABSTRACT:

A complex quasi wavelet basis function for time-frequency analysis is proposed, and the associated numerical processes are explained. Using a scheme similar to the continuous wavelet transform, the function basis yields informative features both in the modulus and phase plane renditions. Various simulated and experimental signals are used to validate its serviceability, in particular, the extraction of instantaneous frequencies or the power ridges of a signal. The results are also compared to those of the Morlet wavelet, and they show the superiority of the present basis function. Analytical aspects of the behaviors of the devised basis, such as frequency leakage-in or leakage-out, ambiguity effects, phase noise, and the criteria of local power extremes, are also studied and compared to the corresponding counterparts of the Morlet wavelet. And these characterizations manifest the usefulness and superiority of the present function basis, as well as its practical applicability.

DATE OF PUBLICATION	NUMBER OF PAGES	PRICE	CLASSIFICATION
April 2006	86	100	☐RESTRICTED ☐CONFIDENTIAL ☐SECRET ☐TOP SECRET ▒UNCLASSIFIED

訊號分析法比較研究
暨其於水波應用探討—
新型類仔波函數及其
時尺轉換特性與應用

Time-Frequency Analyses and Their Applications — A Quasi Wavelet Basis Function for Improved Time-Frequency Characterizations

李 勇 榮

交通部運輸研究所港灣技術研究中心

Email: ronlee@ms4.hinet.net

Revision: 1.0, March 20, 2006, 01:06:56

Printed: March 21, 2006

LIST OF CONTENTS

LIST OF FIGURES

LIST OF TABLES

摘要

本文提出一新型類仔波複數函基函數，並說明其模值與相位之介定與數值求取方式。此類仔波於時頻分析瞬間頻率之擷取或能脊線分佈之檢測上具有較莫利仔波更爲明確容易之優越性。此外，其模值與相位時尺分佈圖均可提供有義訊息。文中以各種模擬訊號及水槽試驗水波訊號來驗證與比較。另亦探討其表現之各項相關學理因子，如頻漏現象、模糊效應、相位糙訊、能脊規範等。也因爲這些特性，其優異功能得加以解說，而其應用得以突顯一些物理表徵。

ABSTRACT

A complex quasi wavelet basis function for time-frequency analysis is proposed, and the associated numerical processes are explained. Using a scheme similar to the continuous wavelet transform, the function basis yields informative features both in the modulus and phase plane renditions. Various simulated and experimental signals are used to validate its serviceability, in particular, the extraction of instantaneous frequencies or the power ridges of a signal. The results are also compared to those of the Morlet wavelet, and they show the superiority of the present basis function.

Analytical aspects of the behaviors of the devised basis, such as frequency leakage-in or leakage-out, ambiguity effects, phase noise, and the criteria of local power extremes, are also studied and compared to the corresponding counterparts of the Morlet wavelet. And these characterizations manifest the usefulness and superiority of the present function basis, as well as its practical applicability.

Chapter 1

Introduction

The core of signal analysis is the study of analyzing function bases and their relevant numerical processes. And we also know that the usefulness of an analyzing function basis and its relevant numerical process is mostly signal-dependent and purpose-oriented. For example, from the perspective of image or acoustic signal processing, the aim may mainly focus on transform compactness, speed efficiency and fidelity restoration, and here physics plays a lesser role in our concerns. While, from the perspective of water wave signal analysis, the aim may exclusively focus on the disclosure of physics, and here speed and compactness are surely trivial. The basic simple fact is that there is neither a general basis that is optimum for all applications nor a general scheme that best appeals to all circumstances.

Time-frequency analysis is the study of time-varying spectra of signals and it involves a vast array of methods. Different methods yield different results, and the results may sometimes seem irrelevant, and quite often at odds with each other. It is therefore never too cautious to be prudent in making interpretations.

Conceptually, a time-frequency transform is the projection of a target function (or a signal) into the basis functions of a certain function basis (i.e., the set of basis functions) mainly for characterizing the non-stationary features of that target function. In this regard, from the physical perspective of water wave signals, it is intuitively right to think of the study as the pursuing of a function basis that provides the best match among the basis functions and the "intrinsic" signal constituents. However, a prior note is that the present study concerns a function basis that does not conform to such a thinking; nevertheless, it provides useful information concerning time-scale characterizations of signals.

The windowed Fourier transform (or short-time Fourier transform) and the wavelet transform are the two commonly seen methodologies of time-frequency analysis. In the former, the transform basis is comprised of windowed Fourier eigenvectors; in the latter, the transform basis is formed by wavelet atoms that are the scaled and translated versions of a mother wavelet.

Ideally, one would like to have a transform that does not spread energy of any constituent signal component in both the time and frequency (or time and scale) domains. Or desirably, the transform should yield time-frequency distributions that have minimum ambiguity or interference due to time and frequency spreading of component signals or Fourier components. However, the theoretical restriction of the Heisenberg uncertainty principle, as well as the many lingering paradoxes (such as negative frequency, negative power, unallocated frequency components, etc.) arising from various time-frequency analyzing kernels, has dictated that the ambiguity and the interferences can never be completely or simultaneously removed. Hence, one always has to live with the trade-offs among different bases and different approaches, and constantly be aware that false and intractable, or isolated and unrepeatable, interpretations may be at large.

In this study we proposed a new complex basis function, and through employing the numerical scheme similar to that of the continuous wavelet transform we study the nature of the basis function and characterize both simulated data and experimentally acquired water wave signals. In contrast to most studies of other bases, we put equal emphasis on the modulus and the phase plane information, and show they both are informative.

We also note that, in a strict sense, the present basis function may lack mathematical rigorousness in a few analytical aspects, such as sufficing the concepts of Hilbert space, serving as a tool for the characterization of local regularity, and building useful operators related to the resolutions of the identity, etc. But the hardheaded fact, in a pragmatic sense, is its ability to provide richer information than can other bases, such as those associated with the continuous and the discrete wavelet transforms. It is therefore natural to compare our results to those of the Morlet wavelet that is typically used in water wave applications.

In a further attempt to reveal the inner working of the proposed basis function, a few analytical aspects that manifest the behaviors of the devised basis, such as frequency leakage-in or leakage-out, ambiguity effect, phase noise, and the concepts of local extremes, will also be studied. And again, these features are compared to those corresponding counterparts of Morlet wavelet.

Judging from the numerical methodology adopted, as well as considering the above mentioned lack of inherent rigorousness, it may be appropriate to regard the present basis function as a "quasi" wavelet basis function or as a wavelet variant. Therefore, more emphases should be placed on the variant's practical usefulness in applications rather than on its fulfillments of various mathematical constraints. However, we shall somewhat follow the formalism of time-frequency analysis in characterizing the cause-and-effect phenomena and acquaint ourself with analytical countenance and applied demeanors, so as to be guided towards possible new efforts. ❖

Chapter 2

The Quasi Wavelet Basis Function

2.1 Introduction

For the studies of water wave related signals using wavelet approach, avery important factor that contributes to the usefulness of a wavelet function basis in revealing the most intimately, as well as intricately, physical aspects of the signals is that the function basis should possess the following property: the associated mother wavelet should have "complete oscillation" and the associated scaling function should have "total positivity". Physically speaking, this property means that the basis functions, in comparison with other basis functions, are relatively quite regular. And practically, this means that a transform associated with "complete oscillation" and "total positivity" provides information that is far more tangible than otherwise provided. This further, in more plain language, implies that if there is a slight change in signal content than a basis with such a property will yield transform coefficients that are more or less "reasonably expected" or "mildly altered"; otherwise, the variation of transform coefficients arising from such a slight change may be completely ad hoc [14, 16, 21]. Figure 2.1 well illustrates the above argument and points out the inherent causes related to these phenomena.

Based on the cognition above, as well as from our previous studies on the entropy performances for a comprehensive set of wavelet basis categories, the cardinal spline wavelet has been shown to be exactly the optimum basis for modeling water wave related signals from the point of view of discrete transforms (including the discrete Fourier transform) [15, 21, 16]. And a natural extension of such an optimum basis to the continuous transform thus implies the Morlet wavelet to be a very appropriate candidate, although the Morlet wavelet does not strictly fulfill the conditions of “complete oscillation” and “total positivity”.

With these understandings, we will thus compare the performances and feature outcomes of the present methodology with those of the Morlet wavelet. In brief, what we like to deliver here is that the present methodology not only possesses the same easiness in numerical implementation but also holds an improved capability in extracting constituent power ridges of signals from both the modulus and phase plane renditions.

2.2 The devising of the basis function

For many wavelet analyses, the transforms concern only real basis functions. In such a sense, phase information may be of little concern in certain applications. For time-frequency analyses, although it is possible to express a real signal in real functions of phase and amplitude, it is often advantageous to associate a signal with a complex form and take the actual signal to be the real part of the complex signal. In such a way, a complex basis function provides the advantage of a more natural modulus-phase-form information. It is important to note that the phase and amplitude of the real signal are not generally the same as the phase and amplitude of the complex signal.

To take advantage of the modulus-phase information we design the present basis function to be complex and take the time-frequency transform to be fundamentally a wavelet approach. And the basis function $\psi(t)$ is defined as:

$$\psi(t) = \frac{1}{\pi^{\frac{1}{4}}} \left[\operatorname{sgn}(t) \sin \omega_0 t - i \cos \omega_0 t\right] e^{\frac{-t^2}{2}}. \tag{2.1}$$

The function serves as the seed of a function basis in a way similar to what a mother

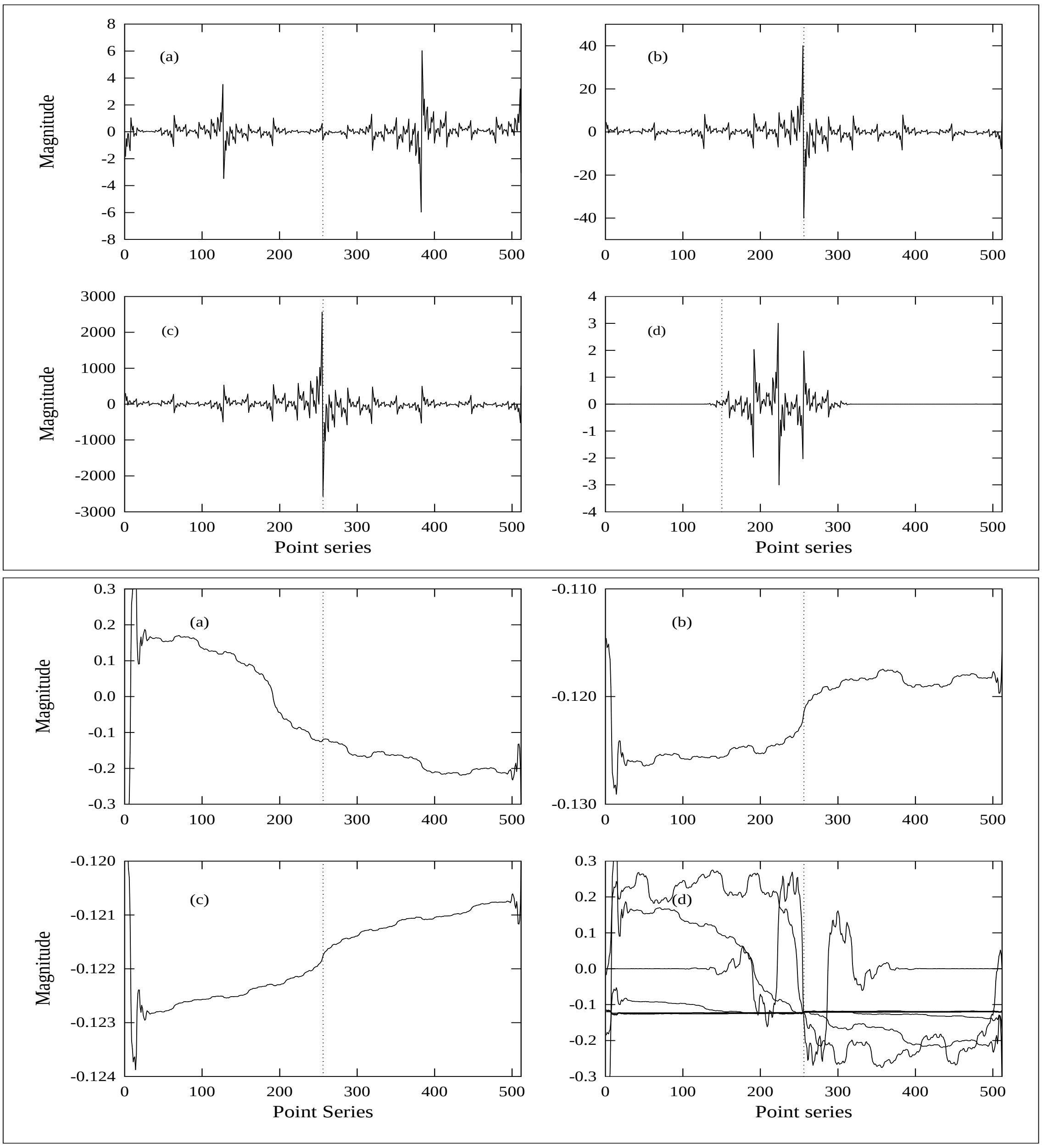

Figure 2.1: Wavelets with fancy analytical properties are often of eccentric wave forms and are not of our choice for studying water-wave related physics — Either judging from their entropy values or form their stability conditions shown here. Here the blow-ups of bi-orthogonal wavelets BO31O and BO35O are shown, respectively, in top and bottom halves of the figure. Related data for BO31O is: {Blow-up point: 150 (located at the dotted line in figure (d)); Origin: level 2, position 12 (i.e., U_2^{12}); Length: 512 (the curve in figure (d)). Figures (a), (b), and (c) show successive blow-up scale of 2^6. The blow-ups diverge rapidly, i.e., the wavelet fails to identify itself numerically in the refinement cascade.} Related data for BO35O is: {Blow-up point: 256 (located at the dotted line in figure (d)); Origin: U_2^{12}; Length: 512 (one of the curve in figure (d) with parts of the curve coincide with parts of the abscissa). Figures (a), (b), and (c) show successive blow-up scale of 2^6. The blow-ups poorly converge but with peculiar inclinations.}

wavelet does. In the equation, ω_0 is relevant to the modulation frequency of the counterpart Gabor transform (or windowed Fourier transform); $\mathrm{sgn}(t)$ is the sign function; the exponential stands for a Gaussian envelope; and, the constant is somewhat related to a unit norm and serves for matching the counterpart constant of the Morlet wavelet. Figure 2.2 shows the real and imaginary parts of the basis function. Here the basis function is entitled with a "quasi" term in the sense that we mentioned earlier (as well as a few factors to be explained in the next chapter). Besides, considering the nature of the present methodology, one may well regard the basis function to be a "wavelet variant". In fact, compared with the simplified form of the Morlet wavelet, the major difference is the presence of the sign function. Figure 2.3 shows the simplified Morlet wavelet.

The scaled and translated versions of the wavelet variant is :

$$\psi_{a,b}(t) = \frac{1}{\sqrt{a}\pi^{\frac{1}{4}}} \left[\mathrm{sgn}(t) \sin \omega_0 \left(\frac{t-b}{a} \right) - i \cos \omega_0 \left(\frac{t-b}{a} \right) \right] e^{-\frac{\frac{t-b}{a}^{2}}{2}}, \tag{2.2}$$

where a is the scale parameter and b is the translation parameter. The $\frac{\omega_0}{a}$ physically means a carrier frequency and is the core target of the transform information. Note that the "scale" or "frequency" ordinate shown in all modulus and phase renditions to be presented in later chapters represents exactly the values of this variable. And this provides easily perceivable physics, as opposite to many studies that adopted the imperceivable scalar "a".

2.3 The renditions of modulus and phase planes

For a lot of wavelet transforms, such as those related to orthogonal, bi-orthogonal, and semi-orthogonal wavelets, as well as the wavelet packets [3, 5, 29, 24], there are only the modulus results since their bases are real. And for bases that are complex, different transform categories or transforms using different bases quite often place different or unequal weights on their modulus and phase renditions; in other words, modulus and phase renditions provide different degrees of significance in feature identification. And most transforms yield trivial phase information. It will be shown that the present function basis yields somewhat equally informative contents from both modulus and phase renditions. For a one dimensional signal the time-frequency rendition can be displayed in 2-D density plot or 3-D perspective view, and we will use either one when suited.

For the present methodology we define the modulus and phase in the following ways.

Let $f(t)$ be a signal function, the modulus of the transform coefficient is defined either as

$$|\langle f(t), \mathbf{I_m}\psi(t)\rangle + i\mathcal{H}\left[\langle f(t), \mathbf{I_m}\psi(t)\rangle\right]|, \tag{2.3}$$

or

$$|\langle f(t), \mathbf{R_e}\psi(t)\rangle + i\mathcal{H}\left[\langle f(t), \mathbf{R_e}\psi(t)\rangle\right]|, \tag{2.4}$$

where $\mathbf{R_e}$ and $\mathbf{I_m}$ represent real and imaginary part, respectively, $\langle , \rangle$ means the inner product, and $\mathcal{H}$ stands for the Hilbert transform. Note that the implementation of transform in either definition is based on only real or imaginary part alone. In this sense, the modulus may lack the mathematical formalism of a "basis", but here we first point out that the first definition gives basically the same result as Morlet wavelet's, while the second definition yields information that is especially useful in easy extraction of signal power ridges and that is also superior to what provided by the Morlet wavelet.

As to the phase it is defined as

$$\tan^{-1}\frac{\mathbf{R_e}\langle f(t),\, \psi(t)\rangle}{\mathbf{I_m}\langle f(t),\, \psi(t)\rangle} + \left(\frac{\pi}{2}\ \text{ or }\ 0\right), \tag{2.5}$$

or

$$\tan^{-1}\frac{\mathbf{I_e}\langle f(t),\, \psi(t)\rangle}{\mathbf{R_m}\langle f(t),\, \psi(t)\rangle} + \left(\frac{\pi}{2}\ \text{ or }\ 0\right). \tag{2.6}$$

The difference of the two definitions and the presence of the optional constants will become clear when we come to show the transform planes of phase in the following chapters. Basically the added constant reflects a phase rotation, and they can be used to switch the pattern of significant time-frequency features or to show easy visualizations in accord with either the power ridges of component signals or the time-frequency spreads of constituent components of a signal (or the spreads of basis functions).

The origins and implementations of these definitions will further be explained in the next chapter. Various topics of time-frequency characterizations will also be discussed there. In fact such details are more than practically needed – since if we are merely concerned about the application of a basis, then simply the physical portrayals of modulus and phase suffice to tell all that matter. Nevertheless, we will come to realize that these additional efforts are forthright and warranting, especially when considering that we are making target comparison of performances with the Morlet wavelet (or Gabor short-time Fourier transform), which has well established systematical and analytical exploitations. It is also hoped that by stepping through these characterizations they enhance our understanding of the intrinsic natures or inner workings of any function basis and provides prospects for further investigations.

❖

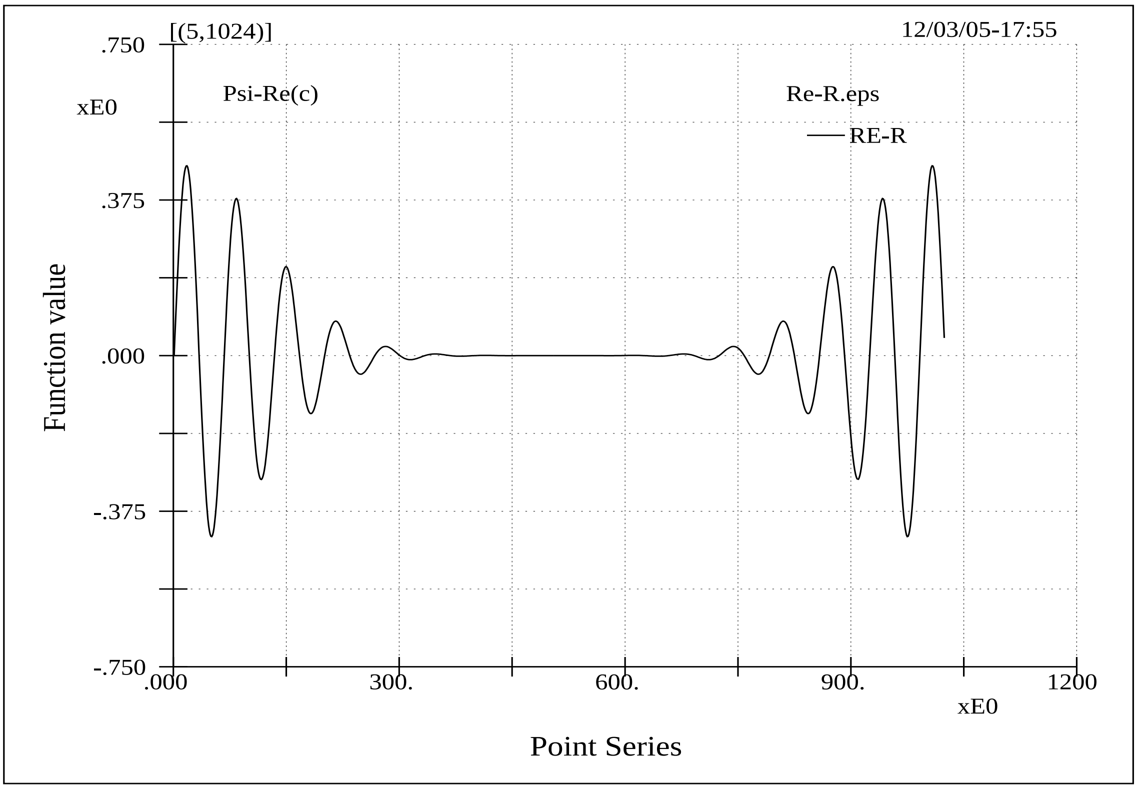

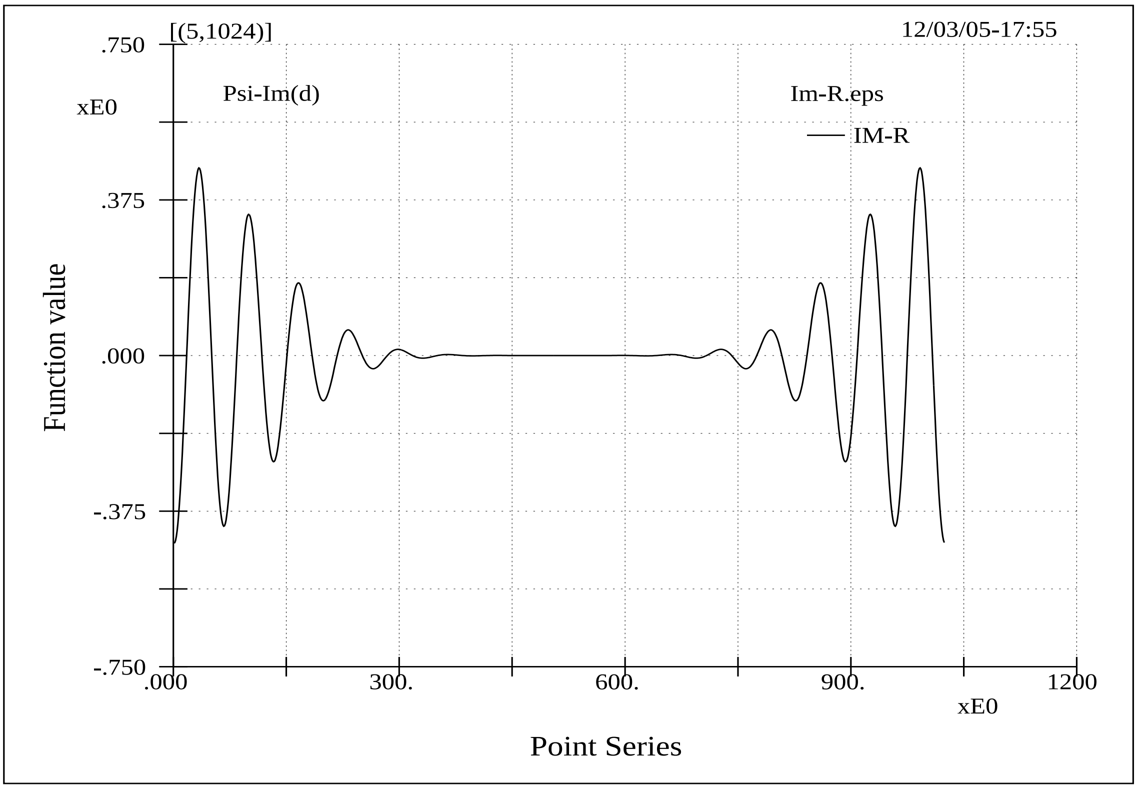

Figure 2.2: The real and imaginary parts of the quasi-wavelet for use in the time-frequency renditions of modulus and phase as defined by equations 2.3, 2.4, 2.5 and 2.6. This quasi wavelet is less analytic than the Morlet wavelet.

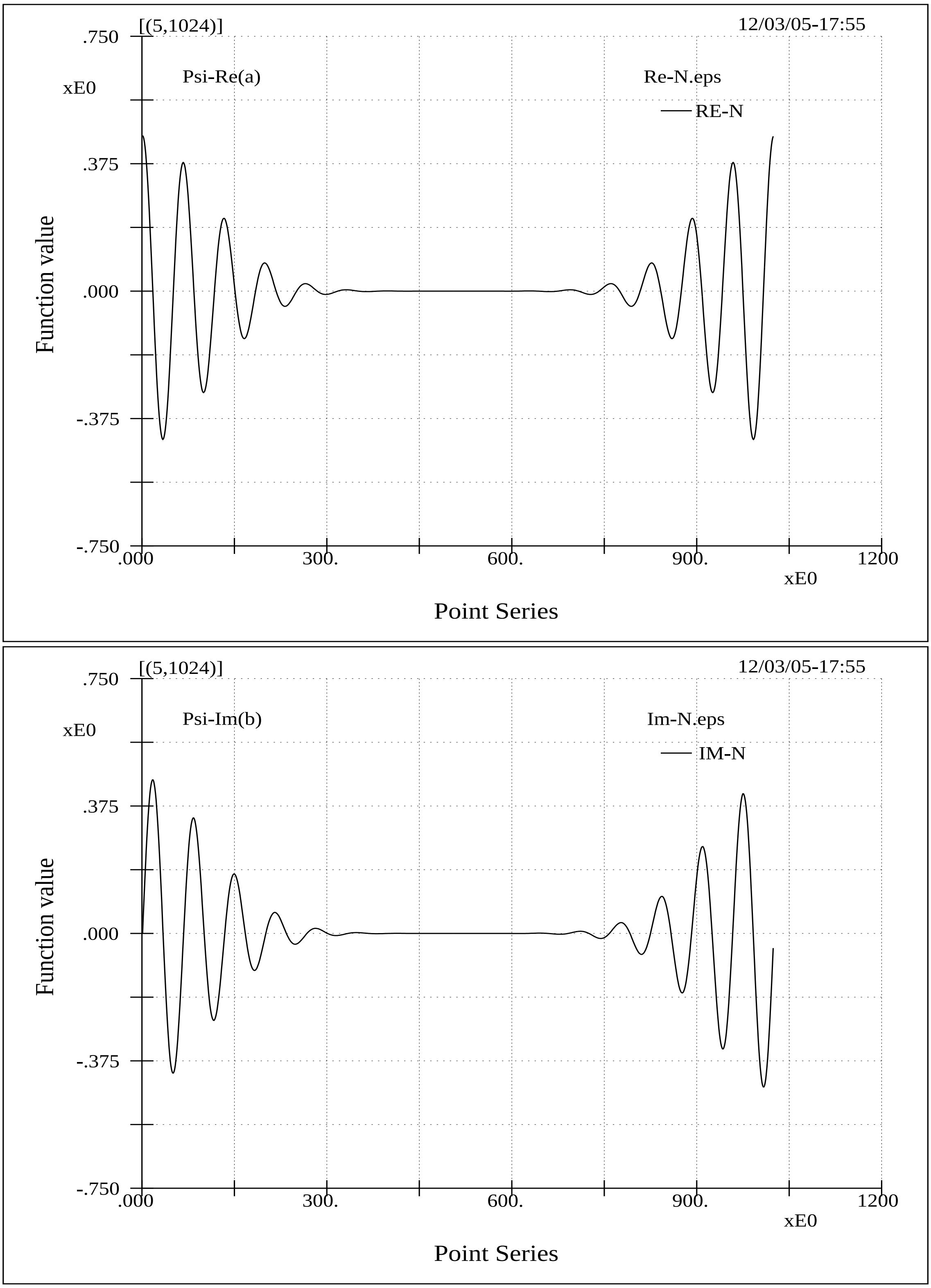

Figure 2.3: The real and imaginary parts of the Gabor type wavelet (the simplified form of Morlet wavelet) for use in the renditions associated with the first definition of modulus (equation 2.3). The wavelet is nearly analytic for most applications when the intrinsic carrier frequencies are not very low.

Chapter 3

Time-Scale Characterizations

3.1 Introduction

Any time-frequency representation – wavelet transform, in a strict sense, is a time-scale representation rather than a time-frequency one – can be associated with a specific auxiliary function, the kernel function. A general class of time-frequency energy density decomposition is the Wigner-Ville distribution. The spectrogram of a windowed Fourier transform, the scalogram of a wavelet transform, and all time-frequency power density distributions derived from some inner product can all be associated with their specific forms of Wigner-Ville distribution [4, 25].

We have not established the association of the proposed basis with a Wigner-Ville distribution, i.e., it is not known whether for any L^2 function one can find its associated Wigner-Ville smoothing kernel or convolution operator. Nevertheless, since we are comparing the results of the present method with those of typical spectrogram or scalogram, we shall, to a feasible extent, follow the formalism of time-frequency and time-scale characterizations so as to make contrasts for the various properties between the proposed quasi-wavelet function basis and that of the Morlet wavelet or Gabor transform. More specifically, the following topics will be considered:

- The wavelet admissibility condition, as well as the concerns about completeness, redundancy, and transform stability;

- The analytic wavelet transform of a real signal and the wavelet transform of the analytic signal, which is complex, associated with that real signal;
- Characterize frequency leakage and phase ambiguity associated with individual basis, as well as illustrate the concepts of time-frequency resolution;
- Compare local power maxima derived from the analytic windowed Fourier transform or wavelet transform to local power extremes, either maxima or minima, derived from the current wavelet variant. In particular, using an analytic signal, we compare its phase and instantaneous frequency as depicted by ridge points in a scalogram or a spectrogram to those as depicted by the present wavelet variant transform;
- Show the phase "randomization" effect in association with an analytic transform and the phase "polarization" effects in association with the present wavelet variant transform;

It is hoped that by these elaborations one can gain basic understanding of the different basis categories, their distinct inherent features, and individual advantages or disadvantages, as well as the "quasi" nature of the proposed wavelet variant basis. And it is also desired that this leads to further cognizance of time-frequency analysis and provides better future prospects in kernel designs.

3.2 The admissibility condition and the completeness and redundancy

If a function $\psi(t)$ is to be qualified as a wavelet for the continuous wavelet transform (CWT), then the only requirement is that $\psi(t)$ meets the following "admissability condition",

$$2\pi \int_{-\infty}^{\infty} \frac{|\widehat{\psi}(\omega)|^2}{|\omega|} d\omega = C_\psi, \tag{3.1}$$

where C_ψ is a constant depending only on ψ only, and $\widehat{\psi}(\omega)$ is the Fourier transform of $\psi(t)$. Among the several definitions of the Fourier transform pairs the one adopted here is:

$$\widehat{\psi}(\omega) = \frac{1}{\sqrt{2\pi}} \int_{-\infty}^{\infty} \psi(t) e^{-i\omega t} dt \tag{3.2}$$

$$\psi(t) = \frac{1}{\sqrt{2\pi}} \int_{-\infty}^{\infty} \widehat{\psi}(\omega) e^{i\omega t} d\omega. \tag{3.3}$$

The admissability condition is the integration of power spectrum weighted by the inverse of the absolute value of frequency; therefore, to yield a finite value, the wavelet should have little power at low frequency and is totally nil at zero frequency, i.e., the area between the curve and the abscissa integrates to zero. This feature basically states that a wavelet should have reasonable decay or be finitely supported — so, it is a wave-let or a wavelet atom.

As to the origin of the constant C_ψ, it is a natural turnout of the derivation of the completeness (such as in the L^2-space) of the wavelet function basis, i.e., it is a byproduct when proofing the following "resolution of identity" for two functions g and h:

$$\langle g, h \rangle = \frac{1}{c_\psi} \int_0^{\infty} \frac{1}{a^2} \int_{-\infty}^{\infty} \langle g, \psi_{a,b} \rangle \overline{\langle h, \psi_{a,b} \rangle} db da, \tag{3.4}$$

where $\psi_{a,b}(t) = \frac{1}{\sqrt{a}} \psi(\frac{t-b}{a})$ is a dilated and translated version of the mother wavelet $\psi(t)$ with dilation parameter $a > 0$ and $a \in \mathbf{R}$ and translation parameter $b \in \mathbf{R}$. The $\frac{1}{\sqrt{a}}$ is for the normalization of L^2-norm. The $\psi_{a,b}$ satisfies admissability condition too. In general, $\psi(t)$ is normalized such that $||\psi(t)|| = 1$; therefore, $\psi_{a,b}(t)$ also has a unit norm.

The admissability condition is a very loose constrain; it does not provide a clear concept of redundancy concerning applying CWT to either discretely sampled or continuous signals. To illustrate this redundancy, let us use the discrete wavelet frame (since the frame wavelet certainly qualifies as a wavelet for CWT): $\psi_{a_0,b_0;j,k}(t) = {a_0}^{-j/2} \psi(a_0^{-j} t - kb_0)$, where a belongs to the set of discrete dilations a_0^j and b to the set of discrete translations

$a_0^j k b_0$; $j, k \in \mathbf{Z}$; and $a_0 \neq 1$ and $b_0 > 0$ are fixed positive constants. For such a discrete wavelet frame we need to impose a more restrictive condition on $\psi(t)$ for its admittance, i.e., the stability condition,

$$b_0 A \leq 2\pi \sum_{j \in \mathbf{Z}} |\widehat{\psi}(a_0{}^j \omega)|^2 \leq b_0 B, \tag{3.5}$$

where A and B are positive constants and $0 < A \leq B < \infty$. The fixed constants b_0 and 2π are intentionally kept since they are related to a normalized wavelet basis and since the magnitudes of A and B are related to the redundancy of the basis. The stability condition may look abstract, but we give its physical implication as: in order for a function to be reconstructed from its wavelet coefficients, i.e., the operation is reversible, we need a process which is convergent when summing all its scales or frequency components. It is therefore necessary that the sum of the power of all the constituent elements can neither be nil or infinity. If the sum is zero, then the elements are all of zero measure — nothing exists. If the sum is infinity, then the elements are significantly overlapping in time and frequency — there is either too much dependence or too much ambiguity and tangling (just like two vectors paralleling to each other do not constitute a good vector basis in two dimensional vector space). If the basis functions are normalized and the inequality of the stability condition are optimized for both the greatest lower bound and the lowest upper bound, i.e., when A and B are defined as

$$A = \inf \left[\frac{2\pi}{b_0} \sum_{j \in \mathbf{Z}} |\widehat{\psi}(a_0{}^j \omega)|^2 \right], \tag{3.6}$$

$$B = \sup \left[\frac{2\pi}{b_0} \sum_{j \in \mathbf{Z}} |\widehat{\psi}(a_0{}^j \omega)|^2 \right], \tag{3.7}$$

then an indication of the redundancy is the average value of A and B, $\frac{A+B}{2}$, supposed that A and B are close to each other (almost tight). If $A = B = 1$, then the basis is orthonormal, and the transform coefficients are without redundancy. Based on this understanding we know that even a mother wavelet of an orthonormal Riesz basis will produce a redundant system when it is applied in the continuous sense. Therefore, continuous wavelet transforms are always redundant when applied to discrete signals and are complete when one likes to increase the resolution indefinitely.

Now let us state a few corresponding attributes of the proposed basis function. Since neither the real nor the imaginary part of the basis function integrates to a zero value, the formula does not satisfy the wavelet admissibility. Therefore, the basis function is really not a wavelet, and this is the main reason why it should be attributed the "quasi" nature at best. Nevertheless, from practical point of view, both the real and imaginary parts do decay as exactly as those of the Morlet wavelet. Here we also note that in common applications a simplified version rather than its full legitimate form of the Morlet wavelet is generally adopted. Nor does this simplified version satisfy the admissibility condition; in fact it is more of a Gabor type "quasi" wavelet. In short, what we like to make it clear is that practically there is no restraint on its application.

In another perspective, since the new seeding function does not belong to a Hilbert space basis, it really does not mean very much to talk about the "completeness" and "redundancy" of the transform coefficients. However, from continuous transform point of view, the completeness and redundancy are more of theoretical or mathematical interest only since a continuous transform has not any practical value in the inverse transform of a discrete signal. Furthermore, taking into account the fact that all signals more or less embed some uncertainty either arising from noise in experimentation or from unavoidable side effects in modeling, the factor of completeness and redundancy really should not hinder our purpose for visually obtaining transform features. In all here we emphasize the practical usage of a quasi wavelet variant.

3.3 The extractions of power ridges

In this section we discuss the transforms that lead naturally to power ridge extractions. For such a purpose the Morlet wavelet is one of the most qualified candidates. Moreover, the Morlet wavelet play a very unique dual role that no other function has — on the one hand, it is certainly associated with a continuous wavelet transform; on the other hand, it is extremely analogous to the basis of the windowed Fourier transform. That is to say it bridges between the continuous wavelet transform and the windowed Fourier transform, and this enable the transform results to provide many physical or practical explanations concerning physics in the conventional or perceptible sense. And this is the reason that our perception of various time-frequency characteristics can be realized or threaded much more easily, and also the reasons why we will be mostly comparing the feature results of the proposed basis with those of the Morlet wavelet.

This is not only because we have mentioned it quite a lot of times but also because we are basically comparing the features of the proposed basis with those of the Morlet wavelet. Moreover, the Morlet wavelet play a unique dual role that no other function has — it crossovers the border between the continuous wavelet transform and the windowed Fourier transform. Due to this specific property, our perception of various characteristics of time-frequency analysis can be realized or threaded much more easily. Some of its significance in certain applications will also be stated in later sections (a more detail account was given in a previous report by the author [13]).

The Morlet wavelet is complex and is given by

$$\psi(t) = \frac{1}{\pi^{1/4}}(e^{-i\omega_0 t} - e^{-\omega_0^2/2})e^{-t^2/2}, \tag{3.8}$$

in which ω_0 is a constant and the term $e^{-\omega_0^2/2}$ justifies the admissability condition. Its Fourier transform is almost a shifted Gaussian and is given by

$$\widehat{\psi}(\omega) = \frac{1}{\pi^{1/4}}[e^{-(\omega-\omega_0)^2/2} - e^{-\omega^2/2}e^{-\omega_0^2/2}]. \tag{3.9}$$

The constant ω_0 is a modulation (or carrier) frequency and has the physical implication of the amplitude ratio r between the second highest peak and the highest peak of $\psi(t)$, i.e.,

$$r = \psi(t_2)/\psi(0), \tag{3.10}$$

in which t_2 is the abscissa of the second highest peak. The exact value of t_2 may be obtained by solving the transcendental equation numerically. But a fairly good explicit estimation can be given by dropping the second term in the above equation since, for most of the scales that concern us, the second term is generally five order of magnitude less than the maximum value of the first term, i.e.,

$$\omega_0 \approx \frac{2\pi}{t_2} \approx \pi \left(-\frac{2}{\ln r} \right)^{1/2}. \tag{3.11}$$

The higher the ω_0 is, the smaller the ratio r becomes. If ω_0 is constant, then the ratio r for different wavelet dilations or scales keeps constant too.

By dropping the second term of equation 3.8 the $\psi(t)$ is strictly not a wavelet but more of a scaled windowed Fourier atom, and the transform becomes more of a scaled Gabor transform, i.e., the Gabor transform with additional scaling of its Gaussian window function. This basically states the dual role of the Morlet wavelet. From the point of view of discrete numerics, the two transforms might not use the same translation step. For the Gabor transform the step is in linear measure, and for the wavelet transform it is in logarithmic measure. Nevertheless, from a continuous perspective, the sense of translation step is trivial; therefore, they are basically identical except that, in the former, the shape and area of time-frequency windows are kept fixed; and, in the latter, the area is kept fixed but not the shape.

Based on the above understanding, there is a natural way to illustrate various wavelet ridge concepts using the scaled Gabor transform since it provides simple and clear illustrations through its intimate association with an analytic process and since the analytic procedure is earthy to the characterization of ridges. The following section describes these relations.

3.4 The analytic property versus complete oscillation and total positivity

A complex function basis provides frequency information and enables us to study amplitude and phase separately. However, there may exist a deep concern about the existence of negative frequencies. Negative frequencies severely retard our mental realization. A common approach to get round of the negative frequency is to perform an analytic procedure either on the basis or on the signal. And it is generally desired that the basis functions be analytic as much as possible.

Now let us state three fundamentally significant concepts that connect "the analytic property" to "the complete oscillation and total positivity" as stated in the previous chapter. First, the Fourier transform of the product of two functions (such as the product of a signal and a window function) is associated with a linear convolution operator in the operation of its opposite domain; conversely, a convolution in one domain corresponds to a multiplication in the other domain. Therefore, if one can design a frequency window which localizes only in the positive frequency and then multiplies the spectral results of a signal with such a window then we might have the desired analytic signal. Second, since the frequency window must not extend to the negative frequency, its center should lie reasonably away from the zero frequency, i.e., the window distribution curve should decays properly fast toward the zero frequency. Third, for the Fourier transform pair, a shift in one domain is equivalent to an oscillation in the other domain. Combining the above three points we come to comprehend the relation between "being analytic" and "being with complete oscillation and total positivity". Overall, this can be stated as: to have a high analytic degree, the analyzing basis functions should have both reasonable oscillation and high regularity in the time domain such that they are properly narrowly band-limited (or almost narrowly band-limited) in the frequency domain.

The above explanations lead to the basic and important understanding why the modulated Gaussian shape function, such as those of the Gabor function basis and the Morlet wavelet basis, are commonly adopted in analyses of water wave related signals – these basis have the highest possibility in revealing physically meaningful features from the conventional time-frequency viewpoint [19, 13, 25].

Talking about frequency, naturally, it is to be associated with the phase or the phase plane rendition. However, to the author's knowledge, the phase plane information of most transforms is quite often rampant and provides little physical interest. More precisely, it rarely provides easy identification of power ridges, i.e., it does not clearly show the instantaneous frequencies associated with the most significant wave components. Part of the reasons is – the phase (or frequency) should intuitively be more or less independent of amplitude, but in fact it is not – this is also the reason why a phase plane is always fully occupied no matter how insignificant the energy content of a region may be. Figure 3.1 makes example such a feature. It should also be noted that for a lot of time-frequency analyses there is actually very sever interaction (or interference) between amplitude and frequency [4, 15]. And again, this factor brings rampant effects on the pattern of the phase plane.

Now let us state those relevant aspects for our devised basis function as depicted by equations 2.3 through 2.6.

First, concerning the modulus, though our definitions of time-frequency modulus plane involve the Hilbert transform, which is related to an analytic process, the analyzing functions are not necessary analytic. Specifically, equation 2.3 is almost analytic and yields nearly the same results as those of Morlet wavelet. In such cases, the instantaneous frequencies corresponding to the significant constituent components are associated with the ridges of the modulus distribution, i.e., the distribution of local energy peak. As to equation 2.4, it is less analytic; nevertheless, we shall show that it provides a new and improved way for ridge extraction. Furthermore, while the instantaneous frequencies of significant constituent components as depicted by equation 2.3 are associated with the power maxima, those as depicted by equation 2.4 are associated with modulus minima, i.e., local power trough.

Second, concerning the phase, even though the time-frequency phase plane as depicted by equation 2.5 or 2.6 is completely filled with phase values, the equations yield completely different, as well as much regular and informative, patterns as compared to those yielded by other transforms. Specifically, the phase distribution based on the Morlet wavelet transform varies so extremely such that it hardly shows any features of practical significance; in sharp contrast, our phase rendition yields almost polarized phase distribution where significant features are revealed by phase interfaces where the neighboring phases are mostly out of phase by convenient separation distances (such as $\pi/2$, π, $3\pi/2$ or 2π). Furthermore, the phase interface lines may represent either the power ridges or the time and frequency spreads of non-orthonormal basis functions.

3.5 The concepts of stationary phase, instantaneous frequency, and transform ridge or trough

In this section we further study the relationships among instantaneous frequency, stationary phase, ridge, and trough concerning the proposed transform.

Let $g(t)$ be a window function in t domain, and $g(t)$ is centered around $t = 0$ and has unit norm with reasonable decay on its support, i.e., $\widehat{g}(0) = \int_{-\infty}^{\infty} g(t)dt$ is the maximum value of $\widehat{g}(\omega)$ and is of the order of 1 For the window function, the windowed Fourier atom is

$$g_{u,\xi}(t) = g(t)e^{i\theta}. \tag{3.12}$$

The Fourier atom scaled by s is

$$g_{s,u,\xi}(t) = g_s(t)e^{i\theta}, \tag{3.13}$$

where subscripts u and ξ stand for translation and scaling parameters, and $g_s = \frac{1}{\sqrt{s}} g(\frac{t}{s})$ has a support of $g(t)$'s scaled by size s and is also with unit norm.

The scaled windowed Fourier transform of a real function $f(t)$ is

$$\langle f, g_{s,u,\xi} \rangle = \int_{-\infty}^{\infty} f(t) g_s(t-u) e^{-i\xi t} dt. \tag{3.14}$$

Basically, this equation provides what equation 2.3 does. And it is also similar to the Morlet wavelet transform using the simplified form by neglecting its second term.

Since any $f(t)$ can always be expressed as $f = a(t)\cos\phi(t)$, one has [31, 25]

$$\langle f, g_{s,u,\xi} \rangle = \frac{\sqrt{s}}{2} a(u) e^{i(\phi(u)-\xi u)} \left(\widehat{g}\left(s[\xi - \phi^{'}(u)] \right) + \epsilon(u,\xi) \right), \tag{3.15}$$

in which the ϵ is an overall corrective term determined by the following four elements:

- The relative variation of amplitude: $\epsilon_{a,1} \leq \frac{s|a^{'}(u)|}{|a(u)|}$;
- The relative curvature of amplitude: $\epsilon_{a,2} \leq \sup \frac{s^2|a^{''}(u)|}{|a(u)|}$;
- The rate of variation of frequency : $\epsilon_{\phi,2} \leq \sup \left[s^2 |\phi^{''}(t)| \right]$; and
- The effects caused by the high frequency components of the window function, i.e., the extreme of the high end part of $|\widehat{g}(\omega)|$: $\epsilon_g = \sup_{|\omega| \geq s\phi'(u)|} |\widehat{g}(\omega)|$

Now let us state a few definitions. The instantaneous frequency (or, simply, the frequency) is generally defined as the time derivative of phase. And the stationary phase is for

$$\phi(u) - \xi u = 0 \tag{3.16}$$

or

$$\xi - \phi'(u) = 0 \tag{3.17}$$

It is therefore known that the stationary phase points are where the ridge locates. But one must also keep in mind that the $f(t)$ (which can be viewed as a single component or combination of components) needs to fulfill the several restrains about ϵ. In a practical sense, the $f(t)$ should be relatively smooth and regular.

Although the above $f(t)$ is the target function rather than a basis function, we should be able to extend these arguments to the case where the $f(t)$ and $g(t)$ switch their roles – judging from the fact that various time-frequency (or time-scale) transforms are simply implementing a projection mechanism. In fact the scaled Fourier atom $g_{s,u,\xi}(t) = g_s(t)e^{i\theta}$ well follows all such requirements. Overall here we clearly illustrate analytically the uses of "complete oscillation and total positivity" and its relationship with the extraction of ridge.

Now let us discuss the analytic degree as related to equation 2.3.

Here we exploit the difference between $\langle f(t), \mathcal{A}[\psi] \rangle$ and $\langle f(t), \psi \rangle$, where $\psi(t)$ is based on equation 2.3, $\mathcal{A}$ means finding the analytic counterpart, and the simulated signal $f(t)$ is an X-signal (a signal composed of two linear chirps with a cross in frequencies).

The top sub-figure of figure 3.1 shows how analytic the basis is – there is basically no energy distribution except at the top area of high frequency.

In the above description we illustrate the relation between ridge and stationary phase points, and we know there is a strong possibility that the two might not be completely coincided. Now let us discuss the corresponding points as will be depicted by equation 2.4 to the ridge points or the stationary phase points as depicted by equation 2.3. And this is done numerically using the Mathematica programming language. It is calculated that the frequencies at the trough points is equal to $\frac{1}{0.969621}$ the values of the ridge points associated with stationary phase points. Here the ω_0 is taken as the commonly adopted value of 5, but different reasonable ω_0 yield values little different from 0.9696. It is also noted that in all subsequent figures in comparison the values of parameter ω_0 (which may take an adapted value to better fit the physics, such as wave's decay property) are the same.

For equation 2.4, since the corresponding basis function lacks the property of complete oscillation and is poorly analytic, we take a different approach in modulus representation: first, the transform is performed only on the real part of equation 2.1, then the analytic signal procedure is applied to that transform result, and finally the envelope curve of the modulus is calculated accordingly.

In the following section we will focus on the analytic signal procedure; this in turn deals with the Hilbert transform.

As to phase plane information the relevant concepts are states below.

Let suppose we have a real function basis, then we have two ways to derive the phases. One way is to devise an analytic function basis with real and imaginary parts as oppose to a basis with real functions only. The other way is to first convert the real signal into an analytic counterpart signal and then apply the transform of the real function basis. It can be shown that the two approaches yield the same results (see e.g., [25]). For equation 2.3, this is what is performed. But for equation 2.4, the complex basis is directly used.

3.6 The analytic signal procedure and the Hilbert transform

Having stated the usefulness of an analytic signal or analytic function basis in power ridge extraction in association with the Gabor transform and the Morlet wavelet transform, we now work on the contents of such a procedure that aims at finding the analytic counterpart of a function. It will be clear that such a procedure inherently involves the Hilbert transform.

Another direct relevance of this section to the present study lies on the use of the Hilbert transform in equations 2.3 and 2.4, even though the perspective now is not on the relation between instantaneous frequency and the ridge point – since neither the quasi-wavelet meets the basic assumption of being a well band-limited function (as is the case for a Gaussian wavelet) nor its analytic form is provided. Therefore, it warrants for us to work through the details that lead to a very easy implementation of the Hilbert transform. This also helps to illustrate possible difficulties or uncertainties that quite often induce

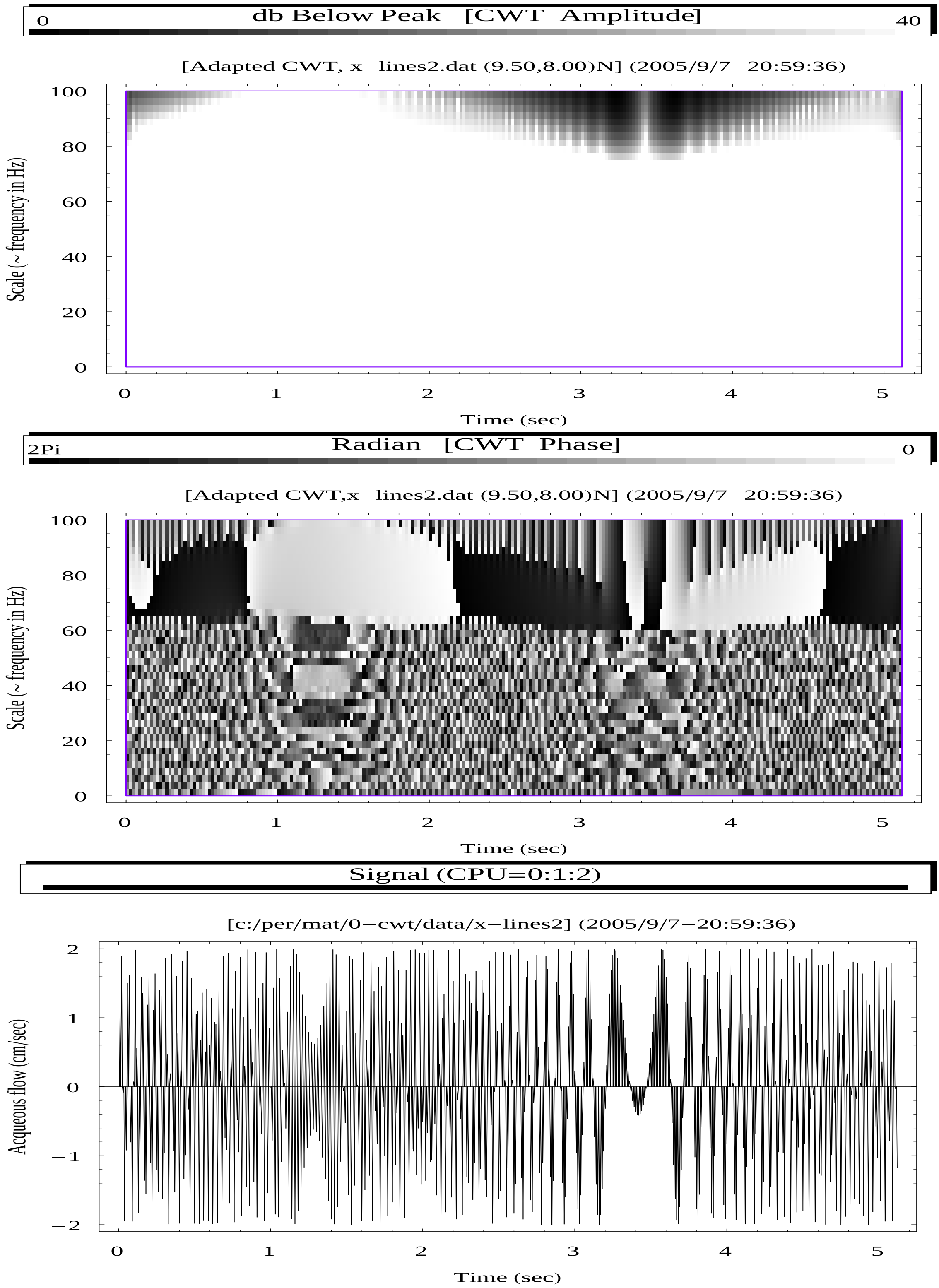

Figure 3.1: This figure shows the analytic degree of ψ related to equation 2.3. The top sub-figure shows the power (modulus squared) of the difference between $\langle f(t), \mathcal{A}[\psi]\rangle$ and $\langle f(t), \psi\rangle$, where $\mathcal{A}$ means the analytic counterpart. The mid sub-figure shows the corresponding phase. Here an X-signal composed of two linear chirps (bottom sub-figure, see figure 4.6) is used.

paradoxes due to non-conformance to the constraints listed earlier.

Let a real signal be $f_r(t)$ and its sensible imaginary counterpart be $f_i(t)$. The real and imaginary parts form a complex signal $z(t)$. A complex function allows us to define its amplitude (or modulus) function $a(t)$ and phase function $\phi(t)$ of a complex exponential. The derivative of the phase yields the natural definition of instantaneous frequency (or local wavenumber in spatial domain) $\omega_i(t)$. The simple mathematical form is

$$z(t) = f_r(t) + f_i(t) = a(t)e^{i\phi(t)}, \tag{3.18}$$

with

$$\omega_i(t) = \phi'(t). \tag{3.19}$$

The main concern here is what is the sensible imaginary part since its choice affects our exploitation of instantaneous frequency. It is appropriate to point out that in the realm of signal analysis most researchers still view the instantaneous frequency as merely a primitive concept rather than a question of mathematical definition. That is to say, the proper definition of the complex signal is still regarded as an open question [4], and the issues are, at best, whether a particular definition can match our intuitive thinking; whether its results can provide adequate explanations for the physics that might be of our own logical reasoning only; or whether the intuitive assumptions induce additional concerns which might be counterintuitive and possibly bring us to new discoveries.

Since any real signal $f_r(t)$ can be expressed as

$$f_r(t) = a(t)\cos\phi(t), \tag{3.20}$$

the most intuitive realization of the complex signal $z(t)$ should be

$$z(t) = a(t)e^{i\phi(t)}. \tag{3.21}$$

Nevertheless, there are infinitely many ways to devise such a complex form. This reflects the openness of the definition of the instantaneous frequency.

In 1946 Gabor [6] proposed a definition for the complex signal that is unique for any real signal and his method is generally referred as the analytic signal procedure.

Let $F_r(\omega)$ be the Fourier transform of $f_r(t)$, the corresponding analytic signal Gabor introduced is,

$$z(t) = 2\frac{1}{\sqrt{2\pi}}\int_0^{\infty} F_r(\omega)e^{i\omega t}d\omega, \tag{3.22}$$

where the factor 2 is introduced so that the real part of the complex signal is equal to the original signal. As is clear from the basic properties of Fourier transform, $z(t)$ must be complex and is the inverse Fourier transform of a single-sided spectrum, which drops the negative frequency components but keeps the same positive spectral components as those of $F_r(\omega)$. Obviously, when the Fourier transform is applied to $z(t)$ again one gets only positive frequency constituents.

Next we illustrate how such a simple complex function can be used to calculate the Hilbert transform of $f_r(t)$. And, in fact, the Hilbert transform is the imaginary part of $z(t)$.

That is to say, we should verify the following identity [4]:

$$z(t) = f_r(t) + i\frac{1}{\pi}\mathcal{P}\int_{-\infty}^{\infty}\frac{f_r(\tau)}{t-\tau}d\tau, \tag{3.23}$$

in which the Hilbert transform of the signal, $\mathcal{H}[f_r(t)]$ is

$$\mathcal{H}[f_r(t)] = \widetilde{f_r(t)} = \frac{1}{\pi}\mathcal{P}\int_{-\infty}^{\infty}\frac{f_r(\tau)}{t-\tau}d\tau. \tag{3.24}$$

In the equation the symbol $\mathcal{P}$ means that the integration is carried out based on the rule of

Cauchy principal value, i.e.,

$$\mathcal{P}\int = \lim_{\epsilon_1=\epsilon_2\to 0}\left(\int_{-\infty}^{t-\epsilon_1} + \int_{t+\epsilon_2}^{\infty}\right). \tag{3.25}$$

Let

$$g(t) = \frac{1}{t}, \tag{3.26}$$

then the Hilbert transform is simply the convolution of $f_r(t)$ and $g(t)$, i.e.,

$$\widetilde{f_r(t)} = \frac{1}{\pi}(f_r \star g)(t). \tag{3.27}$$

By the Fourier duality property, the Fourier transform of the convolution is

$$\mathcal{F}[\widetilde{f_r(t)}] = \widehat{H}(\omega) = \frac{1}{\pi}F_r(\omega)G(\omega). \tag{3.28}$$

Now with $F_r(\omega)$ and $G(\omega)$ being separated the Cauchy principal value operation is related to $g(t)$ only. And the Fourier transform of g is

$$\mathcal{F}[g(t)] = G(\omega) = \mathcal{P}\int_{-\infty}^{\infty}\frac{e^{-i\omega t}}{t}dt = \\ \mathcal{P}\int_{-\infty}^{\infty}\frac{\cos(\omega t)}{t}dt - i\int_{-\infty}^{\infty}\frac{\sin(\omega t)}{t}dt. \tag{3.29}$$

Since the integrant associated with the real part of this equation is antisymmetry the Cauchy principal value integration of this part is zero. As to the integration of the imaginary part, since $\frac{\sin(\omega x)}{x}$ is finite for all values of x, including $x = 0$, there is no need of the principal value sign. Of this part, the integrant is symmetrical; therefore, only half of the integration needs to be considered, and through a change of variable one gets

$$\int_0^{\infty}\frac{\sin\omega x}{x}dx = \mathrm{sgn}(\omega)\int_0^{\infty}\frac{\sin u}{u}du. \tag{3.30}$$

Here one basically know that $G(\omega)$ does not depend on the variation of ω since the integration is independent of ω. Though this integral looks simple, its integration should not be treated as a trivial process; rather, a closed form of the integration can be derived through the use the residue theorem of integration from the complex integral calculus (see for example the well written textbook by Greenberg [7]). The final result is a simple relation which only depends on the sign of ω:

$$G(\omega) = \begin{cases} -i\pi\,\mathrm{sgn}(\omega) & \omega \neq 0 \\ 0 & \omega = 0. \end{cases} \tag{3.31}$$

Accordingly, the Fourier transform of the analytic signal $\mathcal{A}[f_r(t)]$ is

$$\mathcal{F}[\mathcal{A}[f(t)]] = F_r(\omega) + i\mathcal{F}[\mathcal{H}[f_r(t)]](\omega) = \begin{cases} 2S(\omega) & \omega > 0 \\ 0 & \omega \leq 0. \end{cases} \tag{3.32}$$

Here we see that this equation matches exactly with equations 3.22 and 3.23 combined. And it further yields

$$\widehat{H}(\omega) = \begin{cases} -iF(\omega) & \omega > 0 \\ iF(\omega) & \omega \leq 0. \end{cases} \tag{3.33}$$

Making use of this relation the Hilbert transform is easily implemented by a simple word (subroutine) in ASYST language as is shown in Table 3.1.

Detail manipulation of the analytic signal approach is given here not merely for its analytical interest, but rather to disclose its intrinsic nature in association with the Fourier transform properties. An alternative approach implemented in the time domain based on Parks-McClellan minimax algorithm was given in an earlier report on characterizing the amplitude and frequency modulations of water waves measured in laboratory wave tank experiments [12]. In which trade-offs between the two implementations were also illustrated. Here we add one point to the statement given in the introduction chapter – that any numerical scheme is hardly optimum.

As is also indicated in the program one needs to exercise cautions related to non-stationary effects since the basic tactic is related to several simple processes that only manipulate the contents of the FFT of the input signal. And, additionally, we must also acknowledge that the standard deviation of a spectrum is rather significant and its refinement is quite demanding concerning the amount of data points needed.

Overall, here we further illustrate that the ridge algorithm of a Gabor type wavelet transform is only true when the various restraints listed in section 3.5 are obeyed. In analytical term, if we regard the inner product of the transform of equation 3.15 as a linear operator $\mathcal{L}$, then $\mathcal{L}$ must be of a weak continuity, i.e., $\mathcal{L} f(t)$ is modified by a small amount if $f(t)$ is only slightly modified. Thorough numerical experiments on this using laboratory wave data fully support these arguments as are detailed by a previous report by the author [13] (which also includes refined statements for two earlier papers [18, 17] related to the search of an optimum analyzing function basis).

In reality, the above elaborations further manifest an important realization: Due to the fact that the operations associated with orthonormal transforms or any transform that emphasizes efficiency are not in weak form, these function bases just do not provide as much informative physics as what can be provided by the continuous wavelet transform using the Morlet wavelet – Redundancy is sometimes quite helpful [26, 13, 20].

Let us recap the scheme for the definition of equation 2.4. Rather than converting the signal into its analytic counterpart and then projecting it into a real wavelet basis (or rather than directly projecting the real signal into an analytic wavelet basis), the signal is first projected into the real part of the wavelet basis and then the analytic signal procedure is applied to the transform coefficients. In this way the time-frequency power density distribution is obtained as the envelop of the real part wavelet coefficients, i.e., the modulus of the complex transform coefficients.

Table 3.1: An ASYST word, which is equivalent to a subroutine in some computer languages, that performs the Hilbert transform of a signal. This word takes a one dimensional array as the input argument. As seen from the programming, the basic tactic is related to several processes that manipulate the contents of the FFT of the input signal. And because of these manipulations there are endowments of various properties related to FFT into the analytical procedure. In view of the rather significant standard deviation of a discrete spectrum in the Fourier transform, as well as the painfully slow refinement when trying to reduce the value by increasing the amount of data points, the analytic counterpart of a signal quite often possess weird properties, and must be interpreted carefully. Alternatively, these is the implication that the ridge algorithm of a Gabor type wavelet transform is only true when the constraints listed in section 3.5 are obliged.

```
\ ------------------------------------------------------------------------
\  A small program piece which finds the imaginary part of a real signal
\     based on the analytic signal procedure.
\  The computation makes use of the final results of complex calculus based
\     on Cauchy principal value integration.
\  The length of the input array will be automatically truncated to the
\     maximum allowable power of 2.
\ ------------------------------------------------------------------------
: my.hilbert
  fft   []size   n.fft.pts  :=
  dup   becomes>  t1

  dup   sub[ 1 , n.fft.pts  2  /  ]
  0     +1     z=x+iy   *
  t1    sub[ 1 , n.fft.pts  2  /  ]  :=

        sub[ n.fft.pts  2  /  1 +   ,  n.fft.pts  2 / ]
  0     -1     z=x+iy   *
  t1    sub[ n.fft.pts  2  /  1 +   ,  n.fft.pts  2 / ]  :=

  t1   ifft
  zreal
;
\ ------------------------------------------------------------------------
```

3.7 Characterizations of time-frequency resolutions, frequency leakages, and phase ambiguities

The concept of time-frequency resolution basically manifests the principal of Heisenberg uncertainty. This in plain language is to say that since any function can not be finitely supported both in time and frequency domains, the signal, no matter how simple it is, must occupy a finite area in the time-frequency plane – there is no point distribution whatsoever, and so the term resolution. For a basis function, the time-frequency resolution measures its spreads in both time and frequency. And the spreads are generally taken as the second central moments in time and frequency of the basis function. In this sense, if the basis functions are not independent, their time-frequency resolution windows will be overlapping. And this in turn means there are frequency leakage and phase ambiguity. Again the more plain explanation is that one frequency (or one scale, or one basis function) will contaminate all its neighboring frequencies (or other scales, or other basis functions), and any point in the time-frequency plane really is collecting all sorts of distorted energy that belong to its surrounding others. Hence come the terms of frequency leakage-out and -in.

In a practical sense, if the time or frequency distances of the constituent components of a signal are too short, there will be significant overlapping of their energy, and the power of one component might be overshadowed by others. Under such conditions the identification of constituent components will be difficult. It is therefore important for us to characterize the behaviors of frequency leakage and phase ambiguity of the present basis function and compare them with those of other bases, especially, those of the Morlet wavelet.

For equation 2.3 the corresponding basis function is of a modulated Gaussian which has an envelope centered and peaked at zero time, and the basis function has an exact carrier frequency. As for equation 2.4 the corresponding basis function has an envelope which can be treated as either with a singly peaked bump or with doubly peaked bumps according to one's desire whether to pin the envelope curve to the zero center point of the oscillation curve. But here the basis function does not have a real carrier frequency, nevertheless, the oscillation does possess a frequency parameter. Although it is legitimate to use time-frequency resolution windows to characterize the smearing effects both in time and frequency, the more appropriate and intricate way is to discuss in terms of time smearing and frequency leakages either arising from a single basis function or from surrounding basis functions.

Here it should also be emphasized that the more precise term for the present section is about "scale" rather than "frequency" since what we do is basically the projection of a wave packet (rather than a uniform sinusoidal wave) into another wave packet.

Before the illustrating various features of the characterizations. let us first state more clearly the characterization contents.

For frequency leakage-out distribution curve we mean the smearing brought by a unit "scale" (or normalized scale) basis function to its neighboring wave packets of surrounding scales; conversely, there is a frequency leakage-in distribution curve which is induced by neighboring individual scales. For time smearing we mean the ambiguity caused by the phase mismatch between two identical basis functions or wave packets. That is to say, the time smearing distribution curve is calculated by projecting a wave packet into its own time-translated versions.

A program written in the Mathematica language is used to derive these results. The program is appended at the end of this chapter. The algorithms and relevant details are somewhat self-explained in the program.

- For the proposed basis function the closed form representation for the leakage-out is derived as

$$\begin{aligned} P(a,\omega_0) &= \frac{1}{\left(\frac{\left(\frac{1}{a}\right)^2+1}{\omega_0^2}\right)^{0.5}} \left(\frac{1}{2}\left(\sqrt{\frac{\left(1+\frac{1}{a}\right)^2\omega_0^2}{\left(\frac{1}{a}\right)^2+1}}\times\right.\right. \\ &\quad {}_1F_1\left(1;\frac{3}{2};-\frac{\left(1+\frac{1}{a}\right)^2\omega_0^2}{2\left(\left(\frac{1}{a}\right)^2+1\right)}\right)\operatorname{sgn}\left(1+\frac{1}{a}\right)+ \end{aligned}$$

$$\sqrt{\frac{(a-1)^2\omega_0^2}{\left(\left(\frac{1}{a}\right)^2+1\right)a^2}} \times$$
$${}_1F_1\left(1; \frac{3}{2}; -\frac{(a-1)^2\omega_0^2}{2\left(\left(\frac{1}{a}\right)^2+1\right)a^2}\right) \operatorname{sgn}\left(1-\frac{1}{a}\right)+\Bigg)\Bigg), \quad (3.34)$$

in which a is a scale, ω_0 stands for a representative carrier frequency parameter (i.e., $a = 1$) and here it is taken as $\omega_0 = 5$, and the ${}_1F_1$ stands for a hypergeometric function.

- Figure 3.2 shows the frequency leakage-out distribution curve for the proposed basis function. The frequency leakage-out is the projection of the unit scale basis function into its neighboring scales. For $\omega_0 = 5$, the curve has a root (i.e., zero value point) at scale 0.969621 rather than 1. The reason for this is conceptually the same as what was stated in the previous section concerning the corrective term ϵ. Here the most significant features are the location of the zero value modulus (i.e., the root) and the sharp steep slopes at both sides of the root. They make possible the easy identification through sharp contrast of modulus values.

- Figure 3.3 shows the frequency leakage-out distribution curve for basis corresponding to the simplified Morlet wavelet. Again the frequency leakage-out is the projection of the unit scale basis function into its neighboring scales. The curve has no root but it has a peak at scale also near to 1. The weight that centers around the zero derivative peak contributes to a relatively broader leakage of energy into its neighboring scales, and there is no sharp contrast in the modulus values.

- For the proposed basis function, the leakage-out distribution curve has two bumps at opposite sides of the root point; while the Morlet wavelet has a single solid bump. This explains why it is appropriate to investigate time and frequency leakages rather than to use time and frequency resolution windows in discriminating their capabilities in analyses.

- Figure 3.4 shows the frequency leakage-in distribution curve for the present basis function. The frequency leakage-in is the projection of a non-unit scale basis function into the unit scale basis function. This distribution curve shows consistent results with that of the frequency leakage-out. Here the parameter values are the same as those of the previous figures. Here the prominent features are also the zero value root point and the small influences from its surrounding proximity.

- Figure 3.5 shows the frequency leakage-in distribution curve for the simplified Morlet wavelet. Again it shows consistent results with corresponding frequency leakage-out.

- Figure 3.6 shows phase noise or time smearing effects associated with the proposed basis function. The phase noise is caused by the phase mismatch between two identical but translated or shifted basis functions. That is to say, it is calculated by projecting a unit scale basis function into its various time-translated versions. Once more, the prominent feature is the existence of a root at the point of zero phase shift. And again, this zero value and smallness around it provide the very significant contributions to the basis' usefulness. Here the modulus is also doubly peaked at the opposite sides of the zero phase point.

- Figure 3.7 shows phase noise or time smearing effects associated with the simplified Morlet wavelet. The phase noise is calculated by projecting a unit scale simplified wavelet function into its various time-translated versions. There is a peak rather than a root at the center. And the largeness of values around the peak point indicates significant interference from phase. The obvious deduction is the difficulty in getting informative features from the its phase plane rendition, and this is certainly related to the afore-mentioned effects of "randomness".

- Combing all the above depictions, one comprehends the reasons why the proposed basis function is able to be helpful in time-frequency or time-scale characterizations and why it is able to be more informative than the Morlet wavelet. It also becomes clear that, regarding the ridge points, the Morlet wavelet (or the basis function corresponding to equation 2.3) is associated with power maxima; while the new basis (or equation 2.4) is associated with the minimum trough points. It is also noted that that a multiplication factor of about $\frac{1}{0.9696}$ is needed for scale adjustment such as to match the trough point to unit scale location.

- For phase plane representations using the proposed basis function, the following specific properties contribute to the possible usefulness in feature extractions. First, at the zero (or low) value trough point (i.e., root point) either the real or the imaginary part (depending on the choice of a phase datum) is of nil value. Second, the leakages, both in and out, are always in opposite signs with respect to the root point. Third, the root point is a reflection point of the leakage distribution curves. Fourth, different visual patterns might show up through the rotation of phase or by adding a phase datum. Fifth, in general, significant features occur at phase value interfaces that separate the neighboring phases at convenient separation distances. ❖

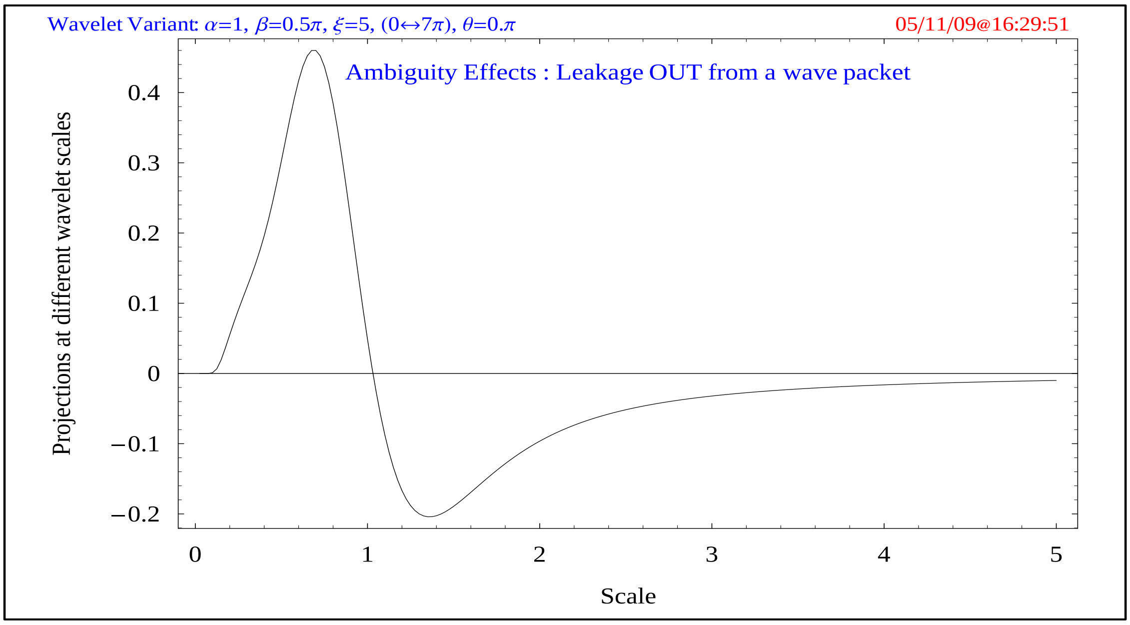

Figure 3.2: The frequency leakage-out distribution curve for the proposed basis function. The frequency leakage-out is the projection of the unit scale basis function into its neighboring scales. For $\omega_0 = 5$ the curve has a root at scale 0.969621. This zero value and the sharp steep slopes at both sides of the root make possible the easy identification of energy ridges.

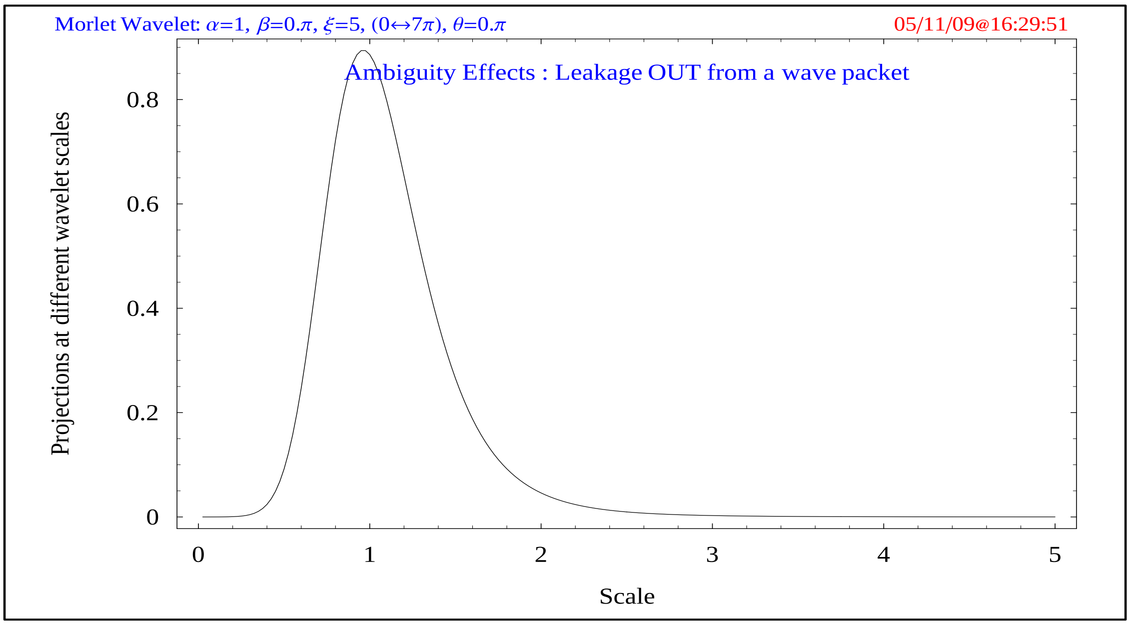

Figure 3.3: The frequency leakage-out distribution curve for the simplified Morlet wavelet. Again the frequency leakage-out is the projection of the unit scale basis function into its neighboring scales. The curve has a peak at scale near to 1. The weight centers around the peak and contributes to a relatively broader leakage of energy.

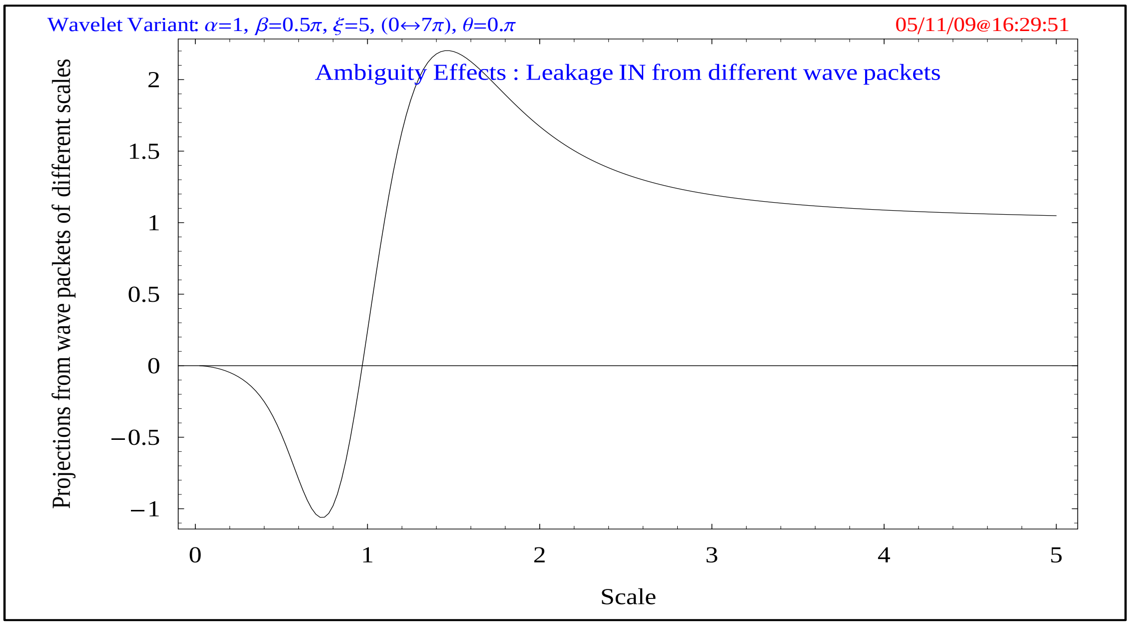

Figure 3.4: The frequency leakage-in distribution curve for the proposed basis function. The frequency leakage-in is the projection of a non-unit scale basis function into the unit scale basis function. It shows consistent results with the frequency leakage-out. Here the parameter values are the same as that of the previous figures.

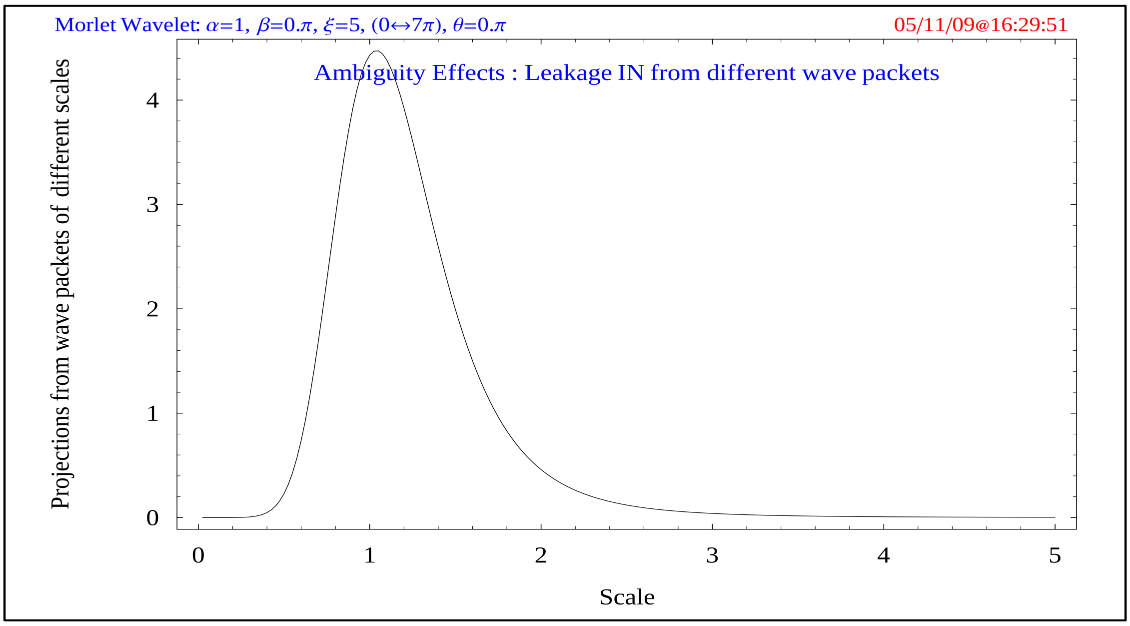

Figure 3.5: The frequency leakage-in distribution curve for the simplified Morlet wavelet. The frequency leakage-in is the projection of a non-unit scale wavelet function into the unit scale wavelet function. It shows consistent results with those of frequency leakage-out.

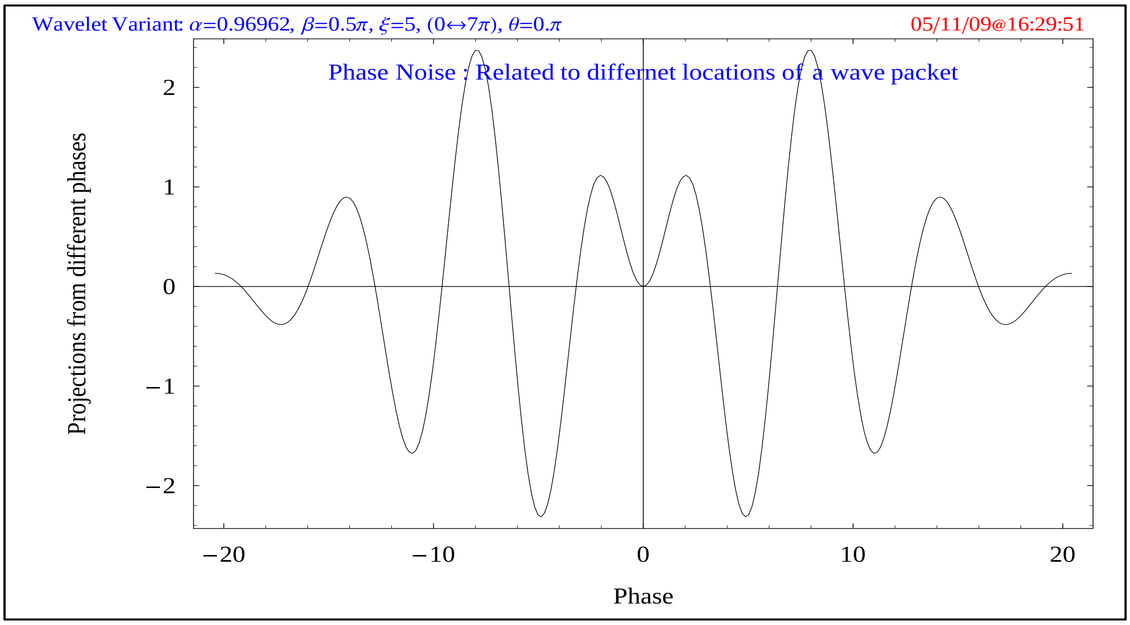

Figure 3.6: Phase noise or time smearing effects associated with the proposed basis function. The phase noise is caused by the phase mismatch between two identical but translated basis functions. That is to say, it is calculated by projecting a unit scale basis function into its various time-translated versions. There is a root at the zero phase point. Again, this zero value and smallness around it provide the reasons for the proposed basis' successful applications using the phase plane information.

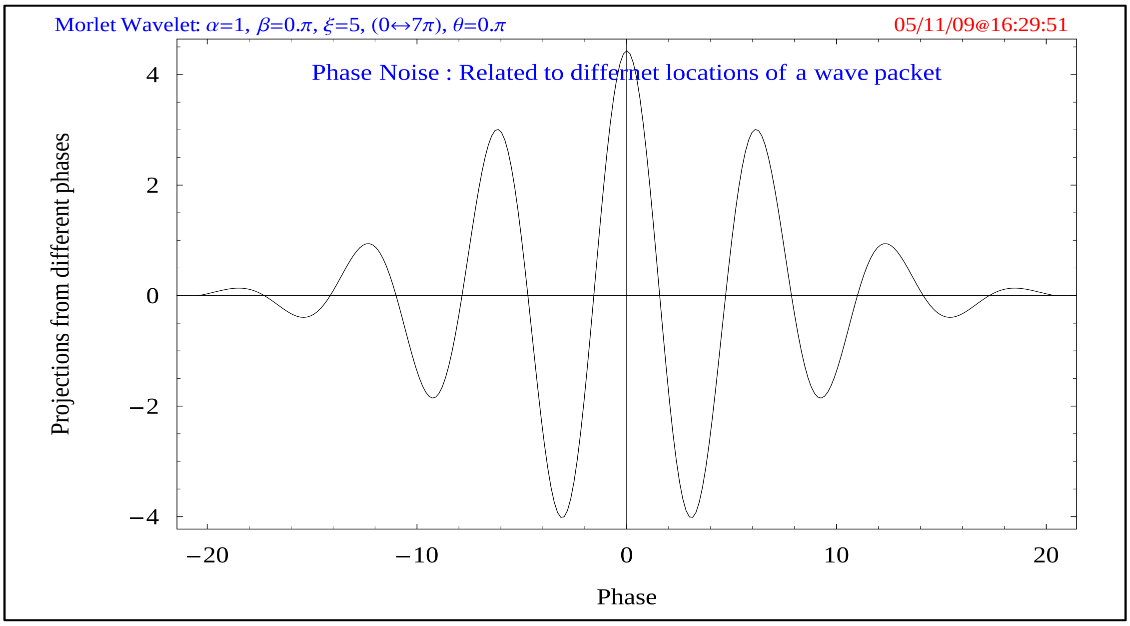

Figure 3.7: Phase noise or time smearing effects associated with the simplified Morlet wavelet. The phase noise is calculated by projecting a unit scale basis function into its various time-translated versions. There is a peak rather than a root at the center. The large values around the center point indicate that it is hard to get informative features from the phase plane information using such a basis.

(* A Quasi Wavelet Basis Function for Refined Ridge Extraction*)

(* by Ron Lee *)

■ Files and Parameters File Macro LeakOut LeakIn PhaseNoise Root Others End

```
<< "c:/lee/mat/Initial_SetNotebook.M" (* Set notebook options *)
<< "c:/lee/mat/Initial_Forms.M";
<< "c:/lee/mat/Initial_Frames.M";
<< "c:/lee/mat/Initial_Words.M";
myfont = "Times";
$TextStyle = {FontFamily -> "Times", FontSize -> myfontsize};
timeflag = "Y";
dynamictimeflag = "N";
flabelflag = "Y";
flabelflag2 = "Y";
abcdflag = "N";
llabelflag = "y";
gridlineflag = "YY";
xyaxisflag = "LL";
stringposflag = 1 ;
xshiftflag = 0;
forcedstringaryflag = "n";
forcedflabelflag = "n" ;
stringindexmul = 3;
stringindexsin = 1;
abcdlabel = "a";
timeflag = "Y"; tlabel = tlabelv;
```

■ Macros File Macro LeakOut LeakIn PhaseNoise Root Others End

```
doshowxy := {
  moutt[flabel];
  moutt[flabel2];
  myplot=ListPlot[ dataxy
    , PlotJoined->True
    , PlotRange->All
    , PlotStyle->{Thickness[0.0008] (* , Hue[0.0] *) }
    , Frame->True
    , DisplayFunction->Identity
  ];
  myshow;
  (* Run["mmawav.bat"]; *)
  <<"c:/lee/mat/000-p2_nb-m.m"
};
```

```
flabel2 := typestr<>"α="<>StringTake[ToString[N[scap1,
9]],If[StringLength[ToString[N[scap1, 9]]]>=7, 7, 1] ]<>", β="<>ToString[N[
peakshiftp1,2]]<>"π, ξ="<>StringTake[
ToString[N[xi,2]],1]<>", (0↔"<>StringTake[ToString[N[xlimitp1, 2]],1]<>"π),
θ="<>ToString[N[phap1,3]]<>"π";
```

- **Leakage Out** File Macro LeakOut LeakIn PhaseNoise Root Others End

- **Leakage out (Wavelet variant)**

```
(* -------- Frequency Leakage Out (Variant) --------- *)
typestr="Wavelet Variant: ";
xlabel="Scale";
ylabel="Projections at different wavelet scales";
flabel="Ambiguity Effects : Leakage OUT from a wave packet";
<<"c:/lee/mat/000-p1_nb-m.m";
frelkgout [peakshiftv_, scav_, xlimitv_, phav_, xiv_] :=
  1 / (scav) * NIntegrate[Cos[xiv*x]*Sin[xiv*x/scav]*
     Exp[-((x - peakshiftv/xiv)^2/scav^2 + (x)^2)/(2)],
     {x, 0, xlimitv}
  , MinRecursion->3, MaxRecursion->10
];
  (*  1 / scav * NIntegrate[Cos[x]*Sin[xiv * x/scav]*   (* a=sca/xi *)
      Exp[-((x/scav - peakshiftv/xiv )^2 + (x)^2)/(2)],
  *)
peakshiftp1=0.5;peakshift= peakshiftp1 * Pi;
xlimitp1=7;xlimit=xlimitp1 * Pi;
phap1=0;pha=phap1 * Pi;
xi=5;
scap1=1;
datax= Table[ ni , {ni, 0.025, 5, 0.025}];
datay= Table[ frelkgout [peakshift, sca, xlimit, pha, xi], {sca, 0.025 ,
5 , 0.025 } ];
dataxy=Table[ {datax[[ i ]], datay[[i]]}, {i,1 ,Length[datax]}];
doshowxy;
```

Ambiguity Effects : Leakage OUT from a wave packet

Wavelet Variant: α=1, β=0.5π, ξ=5, (0↔7π), θ=0.π

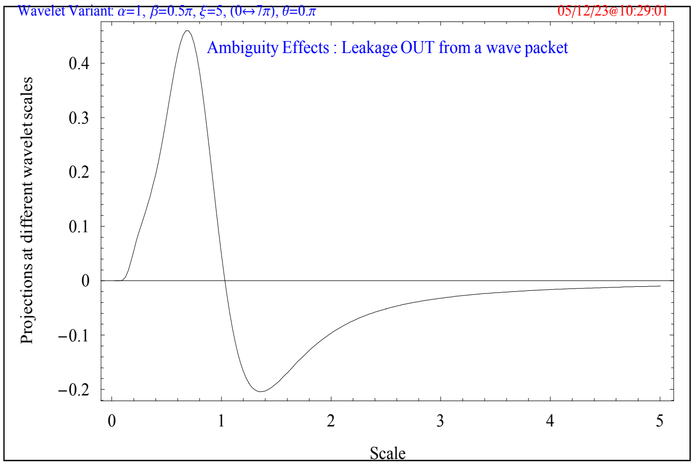

{2005, 12, 23, 10, 29, 1}   CPU:(00, 00, 0.937);   Time:(00, 00, 07)

■ **Leakage out (Morlet)**

```
(* -------- Frequency Leakage Out (Morlet) ---------- *)
typestr="Morlet Wavelet: ";
xlabel="Scale";
ylabel="Projections at different wavelet scales";
flabel="Ambiguity Effects : Leakage OUT from a wave packet";
<<"c:/lee/mat/000-p1_nb-m.m";
(*
frelkginM[peakshiftv_, scav_, xlimitv_, phav_, xiv_] :=
   NIntegrate[Cos[u/scav]*Cos[(u)]*
     Exp[-((u - peakshiftv)^2+ (u/scav)^2)/(2*xiv^2)],
     {u, 0, xlimitv}
     , MinRecursion->3, MaxRecursion->10
];
*)
(*  There exists analytical form  *)
frelkgoutM [peakshiftv_, scav_, xlimitv_, phav_, xiv_] :=
  2*  1 / (scav) * Integrate[Cos[xiv*x]*Cos[xiv*x/scav]*
     Exp[-((x - peakshiftv/xiv)^2/scav^2 + (x)^2)/(2)],
     {x, 0, Infinity}
];
peakshiftp1=0;  peakshift= peakshiftp1 * Pi;
xlimitp1=7;  xlimit=xlimitp1 * Pi;
phap1=0;  pha=phap1 * Pi;
xi=5;
scap1=1;
dofrelkgoutM=frelkgoutM [peakshift, sca, xlimit, pha, xi](*analytical form*)

datax= Table[ ni , {ni, 0.000, 5, 0.025}];
datay= Table[ N[dofrelkgoutM], {sca, 0.000 , 5 , 0.025 } ];
dataxy=Table[ {datax[[ i ]], datay[[i]]}, {i,1 ,Length[datax]}];
doshowxy;
```

$$\frac{1}{sca}\left(2\,\mathrm{If}\left[\mathrm{Im}\left[\frac{1}{sca}\right]==0\ \&\&\ \mathrm{Re}\left[\frac{1}{sca^2}\right]>-1,\right.\right.$$

$$\left.\left.\frac{\left(e^{\frac{25\,(-1+sca)^2}{2\,(1+sca^2)}}+e^{\frac{25\,(1+sca)^2}{2\,(1+sca^2)}}\right)\sqrt{\frac{\pi}{2}}}{2\,e^{25}\sqrt{1+\frac{1}{sca^2}}},\ \int_0^\infty e^{\frac{1}{2}\left(-x^2-\frac{x^2}{sca^2}\right)}\,\mathrm{Cos}[5\,x]\,\mathrm{Cos}\left[\frac{5\,x}{sca}\right]dx\right]\right)$$

Ambiguity Effects : Leakage OUT from a wave packet

Morlet Wavelet: α=1, β=0.π, ξ=5, (0↔7π), θ=0.π

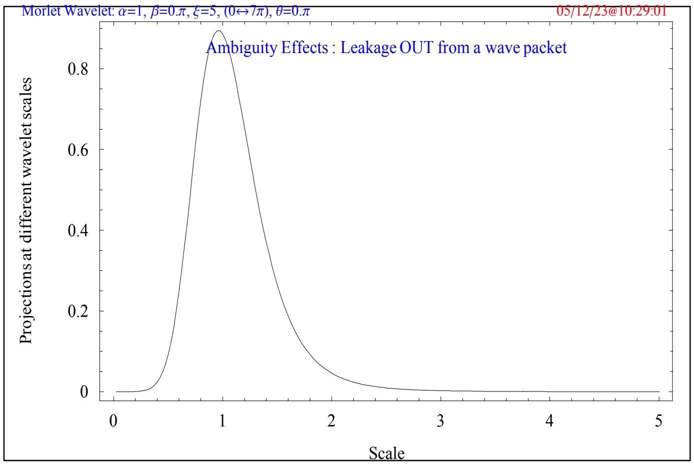

{2005, 12, 23, 10, 29, 8}   CPU:(00, 00, 0.344);   Time:(00, 00, 04)

```
<< "c:\\lee\\mat\\000-p1.m";
```

$$\mathrm{FindMinimum}\left[-1*1/sca*\left(\left(E^{-\frac{25\,(-1+sca)^2}{2\,(1+sca^2)}}+E^{-\frac{25\,(1+sca)^2}{2\,(1+sca^2)}}\right)\sqrt{\frac{\pi}{2}}\sqrt{1+\frac{1}{sca^2}}\,sca^2\right)\Big/\left(2\,(1+sca^2)\right),\ \{sca,\ 0.97\}\right]$$

```
<< "c:/lee/mat/000-p2_nb-m.m"
```

{-0.447397, {sca → 0.962224}}

{2005, 12, 23, 10, 29, 12} CPU:(00, 00, 0.015); Time:(00, 00, 00)

■ **Leakage In** File Macro LeakOut LeakIn PhaseNoise Root Others End

■ **Leakage in (Wavelet variant)**

```
(* -------- Frequency Leakage In (Variant) -------- *)
typestr="Wavelet Variant: ";
xlabel="Scale";
ylabel="Projections from wave packets of different scales";
flabel="Ambiguity Effects : Leakage IN from different wave packets";
<<"c:/lee/mat/000-p1_nb-m.m";
frelkgin[peakshiftv_, scav_, xlimitv_, phav_, xiv_] :=
   NIntegrate[Cos[u/scav]*Sin[(u)]*
     Exp[-((u - peakshiftv)^2+ (u/scav)^2)/(2*xiv^2)],
     {u, 0, xlimitv}
     , MinRecursion->3, MaxRecursion->10
];
(* gsca[b_, a_, s_] := NIntegrate[Cos[u/a]*Sin[(u)]*
                 Exp[-((u-Pi/2.)^2.+(u/a)^2.)/(2*s^2)], {u, 0, b} ] *)
peakshiftp1=0.5;peakshift= peakshiftp1 * Pi;
xlimitp1=7;xlimit=xlimitp1 * Pi;
phap1=0;pha=phap1 * Pi;
xi=5;
scap1=1;
datax= Table[ ni , {ni, 0.025, 5, 0.025}];
datay= Table[ frelkgin [peakshift, sca, xlimit, pha, xi], {sca, 0.025 ,
5 , 0.025 } ];
dataxy=Table[ {datax[[ i ]], datay[[i]]}, {i,1 ,Length[datax]}];
doshowxy;
```

Ambiguity Effects : Leakage IN from different wave packets

Wavelet Variant: α=1, β=0.5π, ξ=5, (0↔7π), Θ=0.π

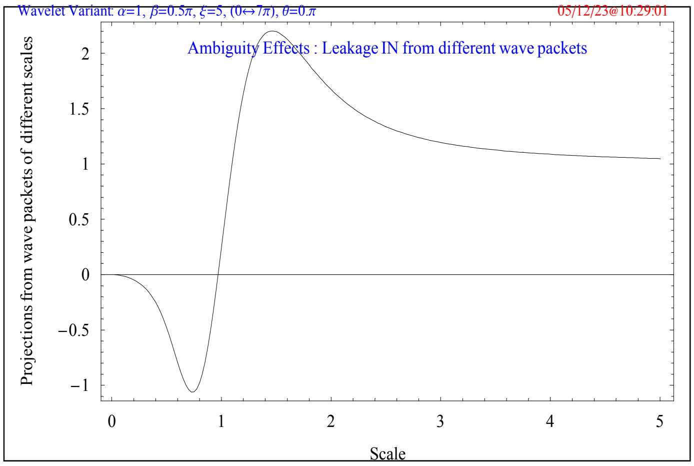

```
        {2005, 12, 23, 10, 29, 12}    CPU:(00, 00, 0.313);     Time:(00, 00,
01)
```

■ **Leakage in (Morlet)**

```
(* --------- Frequency Leakage In (Morlet) --------- *)
typestr="Morlet Wavelet: ";
xlabel="Scale";
ylabel="Projections from wave packets of different scales";
flabel="Ambiguity Effects : Leakage IN from different wave packets";
<<"c:/lee/mat/000-p1_nb-m.m";
(*  There exists closed analytical form  *)
frelkginM[peakshiftv_, scav_, xlimitv_, phav_, xiv_] :=
   2 * Integrate[Cos[u/scav]*Cos[(u)]*
     Exp[-((u - peakshiftv)^2+ (u/scav)^2)/(2*xiv^2)],
     {u, 0, Infinity}
];
peakshiftp1=0;  peakshift= peakshiftp1 * Pi;
xlimitp1=7;  xlimit=xlimitp1 * Pi;
phap1=0;  pha=phap1 * Pi;
xi=5;
scap1=1;
dofrelkginM=frelkginM [peakshift, sca, xlimit, pha, xi](*analytical form*)

datax= Table[ ni , {ni, 0.000, 5, 0.025}];
datay= Table[ N[dofrelkginM], {sca, 0.000 , 5 , 0.025 } ];
dataxy=Table[ {datax[[ i ]], datay[[i]]}, {i,1 ,Length[datax]}];
doshowxy;
```

$$2\,\mathrm{If}\Big[\mathrm{Im}\Big[\frac{1}{\mathrm{sca}}\Big] == 0\;\&\&\;\mathrm{Re}\Big[\frac{1}{\mathrm{sca}^2}\Big] > -1,$$

$$\frac{5\left(e^{\frac{25\,(-1+\mathrm{sca})^2}{2\,(1+\mathrm{sca}^2)}} + e^{\frac{25\,(1+\mathrm{sca})^2}{2\,(1+\mathrm{sca}^2)}}\right)\sqrt{\frac{\pi}{2}}}{2\,e^{25}\sqrt{1+\frac{1}{\mathrm{sca}^2}}},\ \int_0^{\infty} e^{\frac{1}{50}\left(-u^2-\frac{u^2}{\mathrm{sca}^2}\right)}\,\mathrm{Cos}[u]\,\mathrm{Cos}\Big[\frac{u}{\mathrm{sca}}\Big]\,du\Big]$$

Ambiguity Effects : Leakage IN from different wave packets

Morlet Wavelet: α=1, β=0.π, ξ=5, (0↔7π), θ=0.π

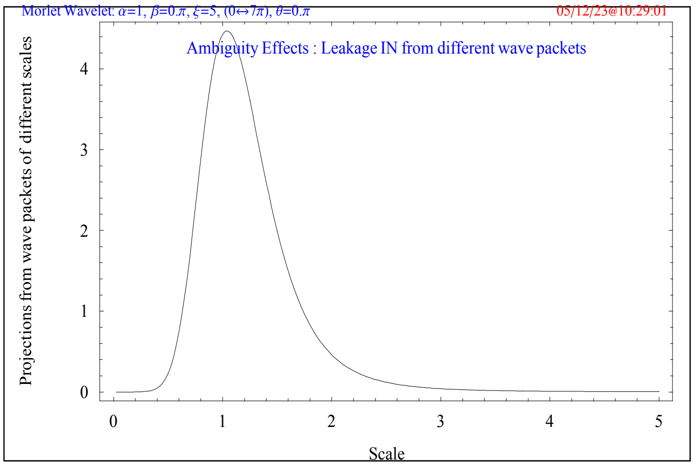

{2005, 12, 23, 10, 29, 13}   CPU:(00, 00, 0.187);   Time:(00, 00, 03)

■ << "c:/lee/mat/000-p1_nb-m.m"

$$\text{FindMinimum}\left[-1 * 10 * \left(\left(E^{-\frac{25\,(-1+\text{sca})^2}{2\,(1+\text{sca}^2)}} + E^{-\frac{25\,(1+\text{sca})^2}{2\,(1+\text{sca}^2)}}\right)\sqrt{\frac{\pi}{2}}\sqrt{1+\frac{1}{\text{sca}^2}}\ \text{sca}^2\right) \Big/ \left(2\,(1+\text{sca}^2)\right), \{\text{sca}, 1.01\}\right]$$

<< "c:/lee/mat/000-p2_nb-m.m"

{-4.47397, {sca → 1.03926}}

{2005, 12, 23, 10, 29, 16}   CPU:(00, 00, 0.);   Time:(00, 00, 00)

■ Phase noise File Macro LeakOut LeakIn PhaseNoise Root Others End

■ Phase noise (Wavelet variant)

```
(* -------------      Phase Noise      --------------- *)
typestr="Wavelet Variant: ";
xlabel="Phase";
ylabel="Projections from different phases";
flabel="Phase Noise : Related to differnet locations of a wave packet";
<<"c:/lee/mat/000-p1_nb-m.m";
integright[peakshiftv_, scaadjv_, xlimitv_, phav_, xiv_] :=
  NIntegrate[Cos[u/scaadjv-phav]*Sin[u]*
    Exp[-((u -peakshiftv )^2. + (u/scaadjv-phav)^2.)/(2*xiv^2)],
    {u, 0, xlimitv}
    , MinRecursion->3, MaxRecursion->10 ];
integleft[peakshiftv_, scaadjv_, xlimitv_, phav_, xiv_] :=
  NIntegrate[Cos[u/scaadjv-phav]*Sin[-u]*
    Exp[-((u + peakshiftv )^2. + (u/scaadjv-phav)^2.)/(2*xiv^2)],
    {u, -1.*xlimitv, 0}
    , MinRecursion->3, MaxRecursion->10 ];
peakshiftp1=0.5;  peakshift= peakshiftp1 * Pi;
xlimitp1=7;  xlimit=xlimitp1 * Pi;
phap1=0;  pha=phap1 * Pi;
xi=5;
scaadj= 0.969621557058245997;  scap1=scaadj;
phaintp1=Table[  integright[peakshift, scaadj, xlimit, phav, xi],
                  {phav, 0.05 Pi,  6.5  Pi , 0.05 Pi } ];
phaintp2=Table[  integleft[peakshift, scaadj, xlimit, phav, xi],
                  {phav, 0.05 Pi,  6.5  Pi , 0.05 Pi } ];
phaintmid=2 * Table[  integleft[peakshift, scaadj, xlimit, phav, xi],
                  {phav, 0.00 Pi,  0.00 Pi , 0.05 Pi } ];
posshiftsum=phaintp1+phaintp2;
midintsum=phaintmid;
datax=Join[ -1* Reverse[Table[ ni * Pi, {ni, 0.05, 6.5, 0.05}]], {0},
Table[ ni * Pi, {ni, 0.05, 6.5, 0.05}] ];
datay=Join[ Reverse[posshiftsum], midintsum, posshiftsum];
dataxy=Table[ {datax[[ i ]], datay[[i]]}, {i,1 ,Length[datax]}];
doshowxy;
```

Phase Noise : Related to differnet locations of a wave packet

Wavelet Variant: α=0.96962, β=0.5π, ξ=5, (0↔7π), θ=0.π

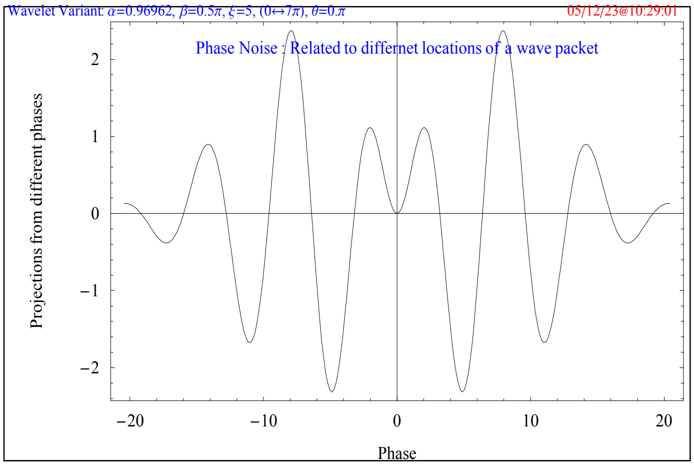

{2005, 12, 23, 10, 29, 17} CPU:(00, 00, 0.454); Time:(00, 00, 00)

■ **Phase noise (Morlet)**

```
(* ---------      Phase Noise (Morlet)     ----------- *)
typestr="Morlet Wavelet: ";
xlabel="Phase";
ylabel="Projections from different phases";
flabel="Phase Noise : Related to differnet locations of a wave packet";
<<"c:/lee/mat/000-p1_nb-m.m";
integrightM[peakshiftv_, scaadjv_, xlimitv_, phav_, xiv_] :=
  NIntegrate[Cos[u/scaadjv-phav]*Cos[u]*
    Exp[-((u -peakshiftv )^2. + (u/scaadjv-phav)^2.)/(2*xiv^2)],
    {u, 0, xlimitv}
    , MinRecursion->3, MaxRecursion->10 ];
integleftM[peakshiftv_, scaadjv_, xlimitv_, phav_, xiv_] :=
  NIntegrate[Cos[u/scaadjv-phav]*Cos[-u]*
    Exp[-((u + peakshiftv )^2. + (u/scaadjv-phav)^2.)/(2*xiv^2)],
    {u, -1.*xlimitv, 0}
    , MinRecursion->3, MaxRecursion->10 ];
peakshiftp1=0.0;  peakshift= peakshiftp1 * Pi;
xlimitp1=7;  xlimit=xlimitp1 * Pi;
phap1=0;  pha=phap1 * Pi;
xi=5;
scaadj= 1;
scap1=scaadj;
phaintp1=Table[  integrightM[peakshift, scaadj, xlimit, phav, xi],
                  {phav, 0.05 Pi,  6.50 Pi , 0.05 Pi } ];
phaintp2=Table[  integleftM[peakshift, scaadj, xlimit, phav, xi],
                  {phav, 0.05 Pi,  6.50 Pi , 0.05 Pi } ];
phaintmid=2 * Table[  integleftM[peakshift, scaadj, xlimit, phav, xi],
                  {phav, 0.00 Pi,  0.00 Pi , 0.05 Pi } ];
posshiftsum=phaintp1+phaintp2;
midintsum=phaintmid;
datax=Join[ -1* Reverse[Table[ ni * Pi, {ni, 0.05, 6.50, 0.05}]], {0},
Table[ ni * Pi, {ni, 0.05, 6.50, 0.05}] ];
datay=Join[ Reverse[posshiftsum], phaintmid, posshiftsum];
dataxy=Table[ {datax[[ i ]], datay[[i]]}, {i,1 ,Length[datax]}];
doshowxy;
```

Phase Noise : Related to differnet locations of a wave packet

Morlet Wavelet: α=1, β=0.π, ξ=5, (0↔7π), θ=0.π

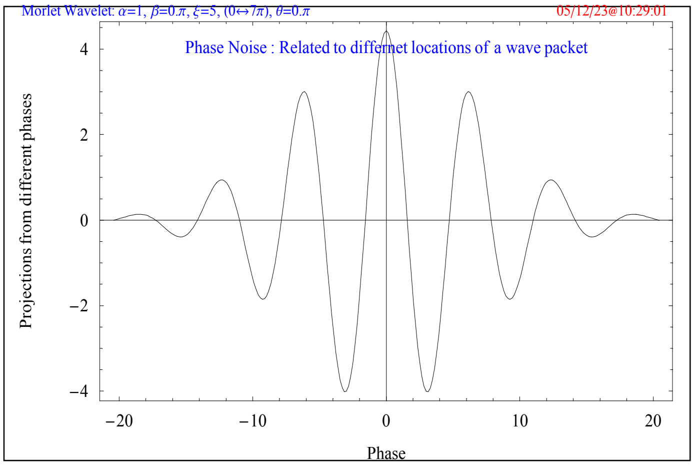

{2005, 12, 23, 10, 29, 17} CPU:(00, 00, 0.468); Time:(00, 00, 02)

■ Roots

File Macro LeakOut LeakIn PhaseNoise Root Others End

```
<< "c:/lee/mat/000-p1_nb-m.m"
g[b_, a_, s_] := Integrate[Cos[u / a] * Sin[(u)] *
        Exp[-((u - Pi / 2.)^2. + u^2.) / (2 * s^2)], {u, 0, b}]
FindRoot[g[5. * Pi, a, 5] == 0, {a, 0.95, 0.7, 1.2}]
<< "c:/lee/mat/000-p2_nb-m.m"
```

{a → 0.970672}

{1998, 7, 27, 2, 18, 16} CPU:(00, 00, 44.27); Time:(00, 00, 44)

```
<< "c:/lee/mat/000-p1_nb-m.m"
g[b_, a_, s_] := Integrate[Cos[u / a] * Sin[(u)] *
        Exp[-((u - Pi / 2.)^2. + u^2.) / (2 * s^2)], {u, 0, b}]
FindRoot[g[7. * Pi, a, 5] == 0, {a, 0.9696, 0.7, 1.2}]
<< "c:/lee/mat/000-p2_nb-m.m"
```

{a → 0.970672}

{1998, 7, 27, 2, 19, 0} CPU:(00, 00, 44.71); Time:(00, 00, 45)

```
<< "c:/lee/mat/000-p1_nb-m.m"
g[b_, a_, s_] := Integrate[Cos[u / a] * Sin[(u)] *
        Exp[-((u - Pi / 2.)^2. + (u / a)^2.) / (2 * s^2)], {u, 0, b}]
FindRoot[g[5. * Pi, a, 5] == 0, {a, 0.97, 0.7, 1.2}]
<< "c:/lee/mat/000-p2_nb-m.m"
(* Run["mmawav.bat"]; *)
```

{a → 0.969622}

{1998, 7, 27, 2, 19, 46}   CPU:(00, 01, 17.17);   Time:(00, 01, 17)

■ Others

File | Macro | LeakOut | LeakIn | PhaseNoise | Root | Others | End

■ Close form integrations

$$g2(b\_, a\_, s\_) = \int_0^\infty \cos\left(\frac{u}{a}\right)\sin(u)\, e^{-\frac{\left(\frac{u}{a}\right)^{2.}+u^{2.}}{2 s^2}}\, du$$

```
<< "c:/lee/mat/000-p1_nb-m.m"
g2[b_, a_, s_] = Integrate[Cos[u / a] * Sin[(u)] *
        Exp[-((u)^2. + (u / a)^2.) / (2 * s^2)], {u, 0, Infinity}]
<< "c:/lee/mat/000-p2_nb-m.m"
```

$$\mathrm{If}\left[\mathrm{Im}\left(\frac{1}{a}\right) == 0 \bigwedge \mathrm{Re}\left(\frac{\left(\frac{1}{a}\right)^{2.}+1}{s^2}\right) > 0,\ \frac{1}{\left(\frac{\left(\frac{1}{a}\right)^{2.}+1}{s^2}\right)^{0.5}}\left(0.5\left(\sqrt{\frac{\left(1+\frac{1}{a}\right)^2 s^2}{\left(\frac{1}{a}\right)^{2.}+1}}\ {}_1F_1\left(1.;\frac{3}{2};-\frac{\left(1+\frac{1}{a}\right)^2 s^2}{2\left(\left(\frac{1}{a}\right)^{2.}+1\right)}\right)\mathrm{sgn}\left(1+\frac{1}{a}\right)+\sqrt{\frac{(a-1)^2 s^2}{\left(\left(\frac{1}{a}\right)^{2.}+1\right)a^2}}\ {}_1F_1\left(1.;\frac{3}{2};-\frac{(a-1)^2 s^2}{2\left(\left(\frac{1}{a}\right)^{2.}+1\right)a^2}\right)\mathrm{sgn}\left(1-\frac{1}{a}\right)\right)\right),\ \int_0^\infty e^{\frac{-\left(\frac{u}{a}\right)^{2.}-u^{2.}}{2s^2}}\cos\left(\frac{u}{a}\right)\sin(u)\,du\right]$$

{1998, 1, 10, 0, 15, 19}   CPU:(00, 00, 15.22);   Time:(00, 00, 15)

$$\mathrm{If}\left[\mathrm{Im}\left[\frac{1}{a}\right] == 0 \,\&\&\, \mathrm{Re}\left[\frac{1+\left(\frac{1}{a}\right)^{2.}}{s^2}\right] > 0,\ \left(0.5\left(\sqrt{\frac{(-1+a)^2 s^2}{\left(1+\left(\frac{1}{a}\right)^{2.}\right)a^2}}\ \mathrm{Hypergeometric1F1}\left[1.,\frac{3}{2},-\frac{(-1+a)^2 s^2}{2\left(1+\left(\frac{1}{a}\right)^{2.}\right)a^2}\right]\mathrm{Sign}\left[1-\frac{1}{a}\right]+\sqrt{\frac{\left(1+\frac{1}{a}\right)^2 s^2}{1+\left(\frac{1}{a}\right)^{2.}}}\ \mathrm{Hypergeometric1F1}\left[1.,\frac{3}{2},-\frac{\left(1+\frac{1}{a}\right)^2 s^2}{2\left(1+\left(\frac{1}{a}\right)^{2.}\right)}\right]\mathrm{Sign}\left[1+\frac{1}{a}\right]\right)\right)\Big/\left(\frac{1+\left(\frac{1}{a}\right)^{2.}}{s^2}\right)^{0.5},\ \int_0^\infty E^{\frac{-u^{2.}-\left(\frac{u}{a}\right)^{2.}}{2s^2}}\mathrm{Cos}\left[\frac{u}{a}\right]\mathrm{Sin}[u]\,du\right]$$

{1998, 7, 26, 17, 28, 31}   CPU:(00, 00, 5.05);   Time:(00, 00, 05)

```
<< "c:/lee/mat/000-p1_nb-m.m"
g3[b_, a_, s_] = Integrate[Cos[u / a] * Sin[(u)] *
        Exp[-((u - Pi / 2.)^2. + (u / a)^2.) / (2 * s^2)], {u, 0, Infinity}]
<< "c:/lee/mat/000-p2_nb-m.m"
```

$$\int_0^\infty E^{\frac{-(-1.5708+u)^{2.}-\left(\frac{u}{a}\right)^{2.}}{2s^2}}\mathrm{Cos}\left[\frac{u}{a}\right]\mathrm{Sin}[u]\,du$$

{1998, 7, 27, 2, 21, 8}   CPU:(00, 00, 8.79);   Time:(00, 00, 09)

Chapter 4

Tests and Applications

4.1 Numerical and experimental signals

Both numerically simulated data and experimentally acquired signals are used to test the performances of the quasi wavelet basis function. In addition, these results are compared to those of the Morlet wavelet. Note that, except otherwise stated, all comparison pairs use the same parameter values.

For numerical experimentation the following simulated signals are used:

- A parabolic chirp with a frequency range of zero to Nyquist rate of 100 Hz;
- A signal composed of two liner chirps that have equal power contents (i.e., the amplitudes are the same) and cross at a frequency point of half of Nyquist rate. It is here denoted as an X-signal;
- An X-signal with a power ratio 0.01 between the two component signals;
- A signal composed of two liner chirps that are parallel (i.e., they are displaced versions in time) and have the same power contents;
- A signal composed of two liner chirps that are parallel but with a power ratio of 0.04.

For practical tests using signals from experiments, water wave signals in laboratory tank either generated by wind or mechanical wave generator are used. They include:

- Short wind waves with respective spectral peaks at about 2.0 to 2.6 Hz;
- Stokes waves with different fundamental harmonic frequencies and different wave steepness values.

4.2 Results and Discussions

- Figures 4.1, 4.2, and 4.3 show the time-scale zoom-ins of the modulus and phase planes of a section of the parabolic chirp with 100 Hz Nyquist rate under several setups, such as, different bases, different numerical resolutions, and different rendering definitions.
- The top two sub-figures in figure 4.1 are the time-frequency modulus and phase renditions, respectively, based on the definition of equation 2.3 or the simplified Morlet wavelet, and there is an indication in the modulus plane that the basis functions are well analytic, i.e., it shows a large blank region. The bottom two sub-figures are associated with the proposed quasi wavelet, and the modulus and phase planes are rendered in accordance with equations 2.4 and 2.5, respectively. It is obvious that the new basis function is able to provide more clear, as well as easier, identifications of the power ridge. That is to say, it is much more convenient to visually obtain the stationary phase points or signal's instantaneous frequencies. Moreover, the phase plane rendered by the quasi wavelet basis function is just as informative as is the corresponding modulus plane. Whereas, it is hard to tell anything physically significant using the phase plane derived from the simplified Morlet wavelet.
- Figure 4.2 also shows the same zoom-in section based upon the proposed quasi wavelet basis function, but here they are associated with different numerical resolutions in scale (or frequency) and also with different adaptations in each scale's time-frequency window (i.e., using different ranges of the parameter ω_0, with small scale a having a larger ω_0 and larger scale a having a smaller ω_0). Even though

here the discrete scale resolution is coarser when compared to that of the previous figure, both the modulus and phase planes still provides very clear features of the instantaneous frequency. In particular, the phase plane renditions show clear interfacial features at all the interfacial points for all the time steps; that is to say, the intermediate time translation points that do not locate at the scale resolution points provides yet the same, as well as very sharp, interfacial features. And this feature is certainly absent in the phase plane rendition using the Morlet wavelet basis.

- Additionally, figures 4.2 and 4.3 shows properties associated with the present quasi wavelet basis function: For example: First, the top and bottom sub-figures of figure 4.2 correspond to equations 2.5 and 2.6, respectively, and they indicate a rotation of coordinate axes; Second, the top and bottom sub-figures of figure 4.3 have a difference in phase equal to a rotation of $\frac{\pi}{2}$ (the constant added to equations 2.5 and 2.6), and the two interfacial phase lines shown in the bottom sub-figure, though a little irregular, well represent the time and frequency spreads (in a sense similar to leakage or ambiguity effects) from the instantaneous frequency curve. Third, the alternating dark-and-light vertical phase strips indicate the cycles of the trough and peak of the signal. Overall, all such phase renditions possess a very distinguish common character that states that significant features occur at interfacial points where the neighboring phases have convenient phase separations such that they are visually in sharp contrast and readily identifiable.

- Figure 4.4 shows the whole extend of the same parabolic chirp for both the simplified Morlet wavelet (the left sub-figures) and the quasi wavelet basis function (the right sub-figures). Again, the phase plane associated with the simplified Morlet wavelet yields little practical significance. Note that there is a slight up-shift of instantaneous frequency for the quasi wavelet basis function, and this up-shift factor is about $\frac{1}{0.9696}$ as derived previously.

- Figure 4.5 shows a zoom-in section of the X-signal composed of two intersecting linear chirps of equal power contents. The left sub-figures are for the simplified Morlet wavelet, and the right sub-figures are for the quasi wavelet basis function. Again, they manifest the same characterizations or comparisons as depicted by those of the parabolic chirp.

- Figure 4.6 shows time-frequency characterizations of the full extend of the same X-signal. The left and right sub-figures are arranged in the same way. Basically they feature identical depictions as those above. One point to note is that around the intersecting region both seem to have distortion. Nevertheless, the proposed quasi wavelet basis function still provides much better information than does the simplified Morlet wavelet. Another point is the existence of the saw-tooth spikes in the 3-D figure of modulus, and these spikes reflect the non-exact match between the instantaneous frequency and the numerical resolution step, and they can be remedied by the phase rendition. Note here that, in the bottom right sub-figure, we have intentionally inverted the rendering, i.e., a trough in the 2-D plane (top right sub-figure) turns to a peak in the 3-D figure; and what is clearly seen is a spike line.

- Figure 4.7 illustrates the effects of phase rotation on the same X-signal based on the quasi wavelet basis function. Again, various interfacial lines in the mid sub-figure serve as indicators of extend of frequency leakage and phase noise. It is noted that the top sub-figure is in color but may here be printed in black and white.

- Figure 4.8 shows the ridge extraction of the signal composed of a pair of parallel chirps with equal power contents. The frequency separation between the two chirps is one tenth Nyquist rate. The left sub-figures are for the simplified Morlet wavelet, and the right sub-figures are for the quasi wavelet basis function. Here we see that the power ridges given by the simplified Morlet wavelet are entirely misleading. Whereas, for the quasi wavelet basis function, the two interfacial lines are clearly identifiable except near the Nyquist frequency. Note here that, in the bottom right sub-figure, what are seen are the two clear spike lines. Undoubtedly, the devised basis function is superior in feature identification.

- Figure 4.9 shows the 2-D and 3-D modulus information of the signal also composed of a pair of parallel chirps but now with difference in power contents, and the energy ratio is 0.04. The left sub-figures are for the simplified Morlet wavelet, and the right sub-figures are for the quasi wavelet basis. In general, both transforms show difficulty in differentiating the two component signals with so large a power difference and so proximate their instantaneous frequencies. Now the weak component signal has been overshadowed by contamination from strong one, and this reflect the combined effects of frequency leakage and phase noise, but one may still say that the right sub-figure is not as distorted as the left one.

- Figure 4.10 shows the time-frequency phase planes for an X-signal that is composed of two component chirps with power ratio of 0.01. The top and bottom sub-figures are associated with the simplified Morlet wavelet and the quasi wavelet basis function, respectively. Again, both have difficulty in rendering any significant feature for the weak component. But still, the quasi wavelet basis function yields unambiguous identification of the strong signal component and is also a bit more informative on the low frequency region for the weak signal.

- Figure 4.11 shows time-frequency features of a water wave signal measured in a wind blowing laboratory tank. The left sub-figures use the simplified Morlet wavelet, and right sub-figures use the proposed basis function. In general the latter ones provide easier and more precise identification of the energy ridge, in particular, the outstanding depictions of its phase plane features.

- Figure 4.12 is associated with the quasi wavelet basis function and shows the time-frequency modulus and phase planes of a water wave signal that is in a lesser developed stage (as referenced to the signal associated with figure 4.11) due to a smaller wind speed in the tank. And the wind wave has a spectral peak located at a higher frequency. A very prominent feature shown in the phase plane is the existence of multiple interfacial points for individual steps along the time line. This strongly reflects the existence of multiple frequency components, as well as indicates the interactions among these components, and it may well serve as the manifestation of water wave modulation phenomena.

- Figure 4.13 compares the time-frequency modulus (top sub-figures) and phase (bottom sub-figures) planes of a mechanically generated Stokes wave using both the simplified Morlet wavelet (left sub-figures) and the present quasi basis function (right sub-figures). Note the Stokes wave has a wave steepness value of about 0.06 for its fundamental harmonic band. Once more, the quasi wavelet basis shows off more interesting physics either from its modulus rendition or phase rendition. First, its modulus plane shows clearly the existence of multi-troughs, and so does its phase plane. Second, both its modulus and phase planes evidence the rapidly oscillating (or up-and-down) interfacial points for the higher frequency trough. Third, for the first fundamental harmonic, the interfacial points of the first half part of the signal are relatively stable and those of its later half get a bit oscillating. In summary, these show wave evolutions and serve as a strong indication of the energy recurrence phenomenon among wave components, as well as of wave evolutions. That is to say, the Benjamin-Feir side-band instability [1, 2, 9, 11, 10, 19, 22, 23, 27, 28, 8, 30, 32] can be featured by the proposed quasi wavelet basis function, and this is generally hard to discern using either the Morlet wavelet or conventional spectral approaches. ❖

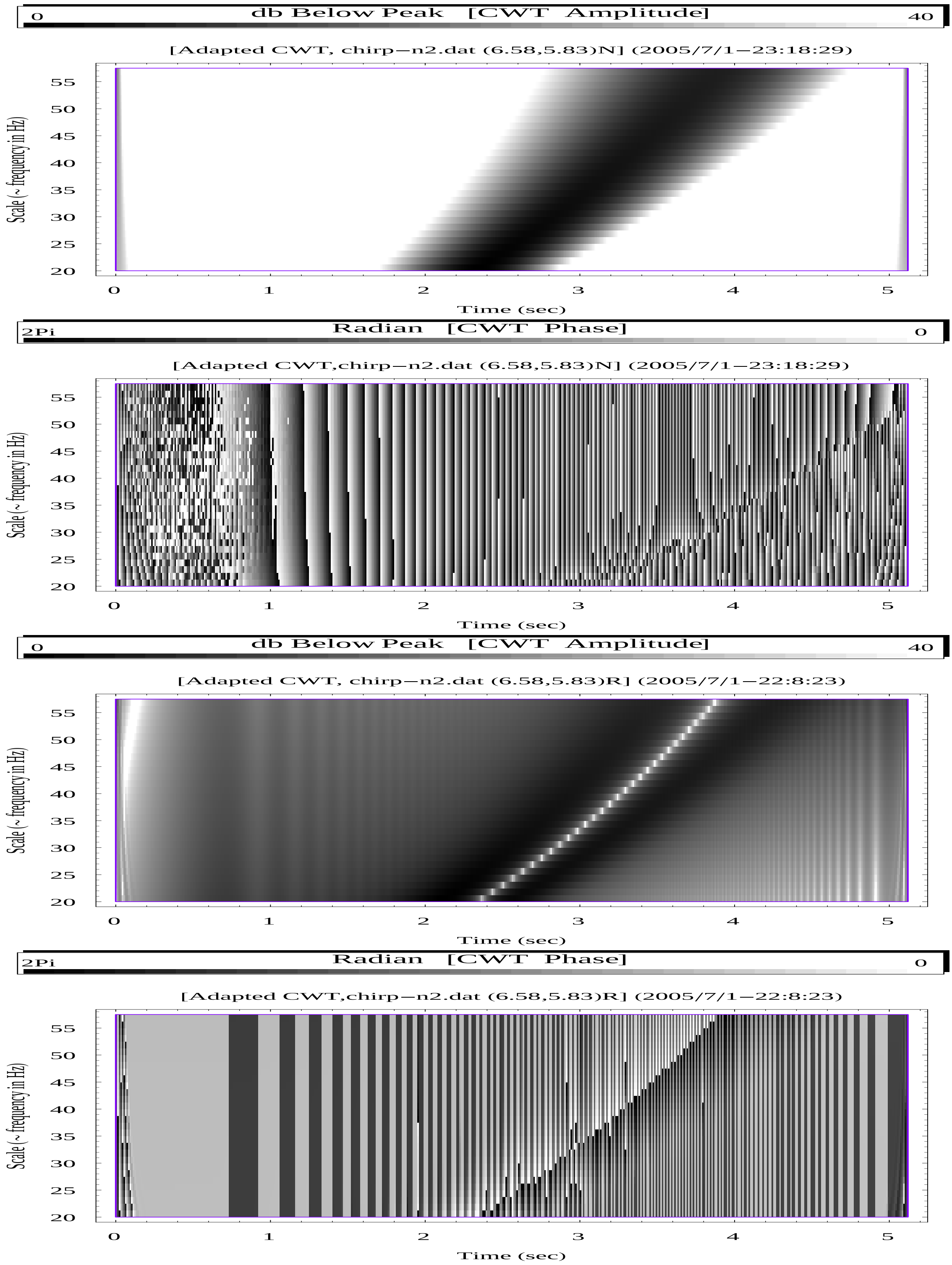

Figure 4.1: The time-Frequency zoom-in of a section of a parabolic chirp with a frequency range of zero to Nyquist rate of 100 Hz. The top two sub-figures are related to the definition of equation 2.3, and it is therefore almost identical to the results of the Morlet wavelet. The bottom two sub-figures are associated with the proposed quasi wavelet basis function (equations 2.4 and 2.5). It is obvious that the proposed function basis provides better and easier identifications of the power ridge or stationary phase points from both the modulus and phase renditions.

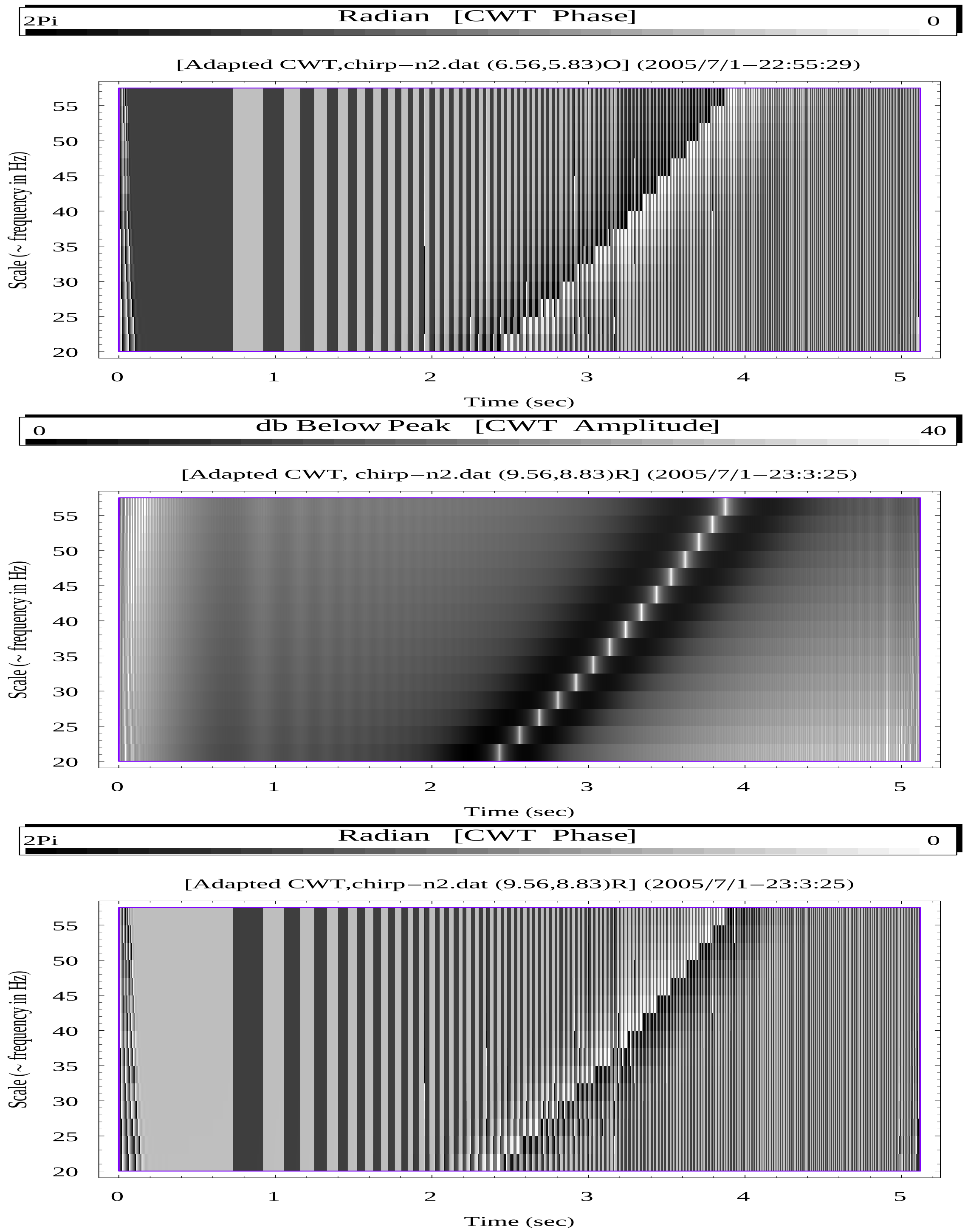

Figure 4.2: The modulus (mid sub-figure) and phase (top and bottom sub-figures) planes for the same time-Frequency zoom-in section using the proposed quasi wavelet basis function, but here the sub-figures are associated with different numerical resolutions in scale and also with different adaptations in each scale's time-frequency windows (i.e., different ranges of the parameter ω_0). Even though the scale resolution here is coarser when compared to that of the previous figure, both the modulus and phase planes still show clear features of the instantaneous frequency. Moreover, the phase plane renditions provides yet the same, as well as very sharp, interfacial features at all the time translation steps, even for those intermediate time translation points that do not locate at the scale resolution points.

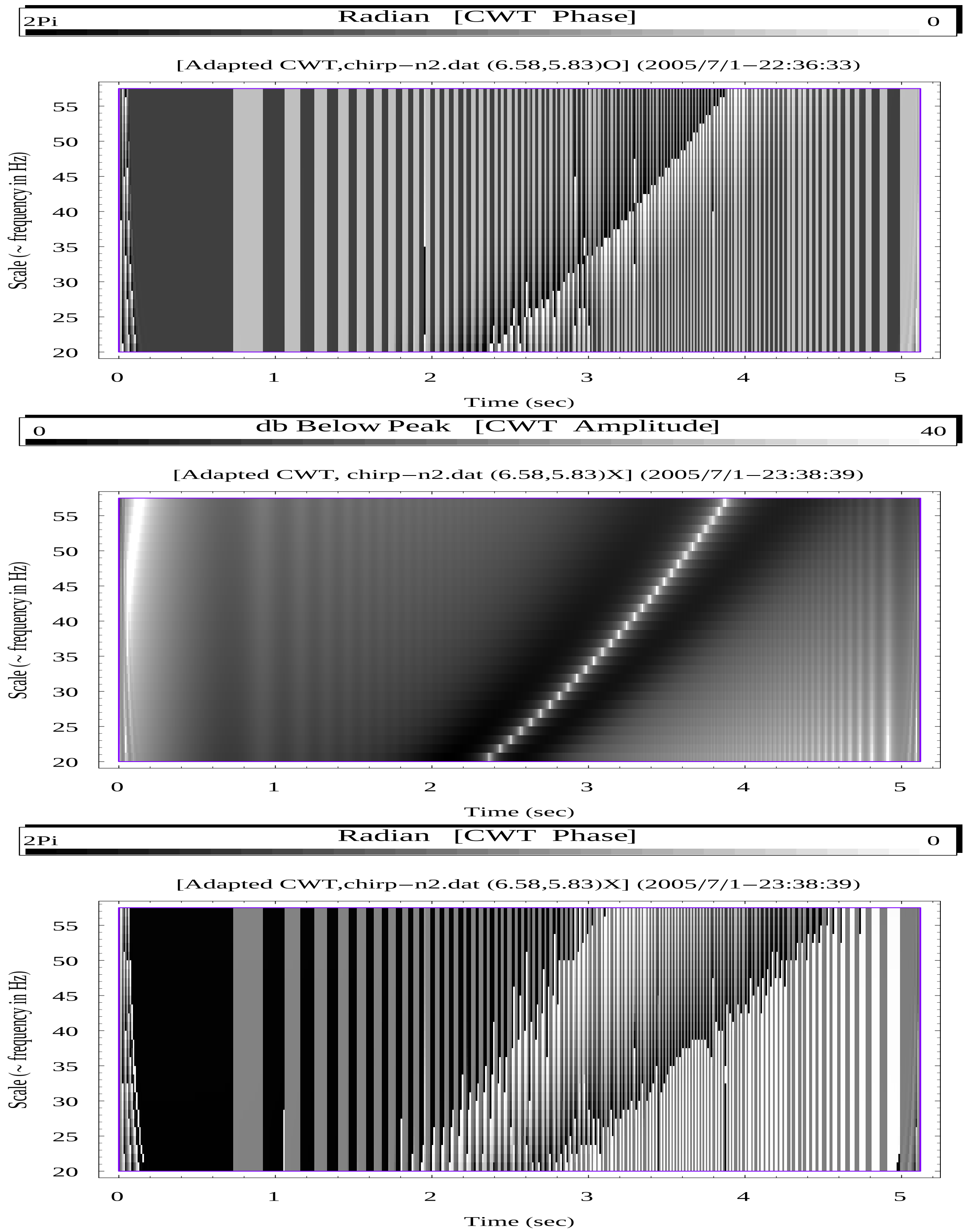

Figure 4.3: This figure shows the effects of phase rotation. The top and bottom sub-figures have a difference in phase rotation of $\frac{\pi}{2}$ (the constant added to equations 2.5 and 2.6), and the two interfacial phase lines shown in the bottom sub-figure represent the time and frequency spreads (in a sense similar to leakage and ambiguity effects) from the power ridge. In addition, the alternating dark-and-light vertical phase strips indicate the cycles of the trough and peak of the signal.

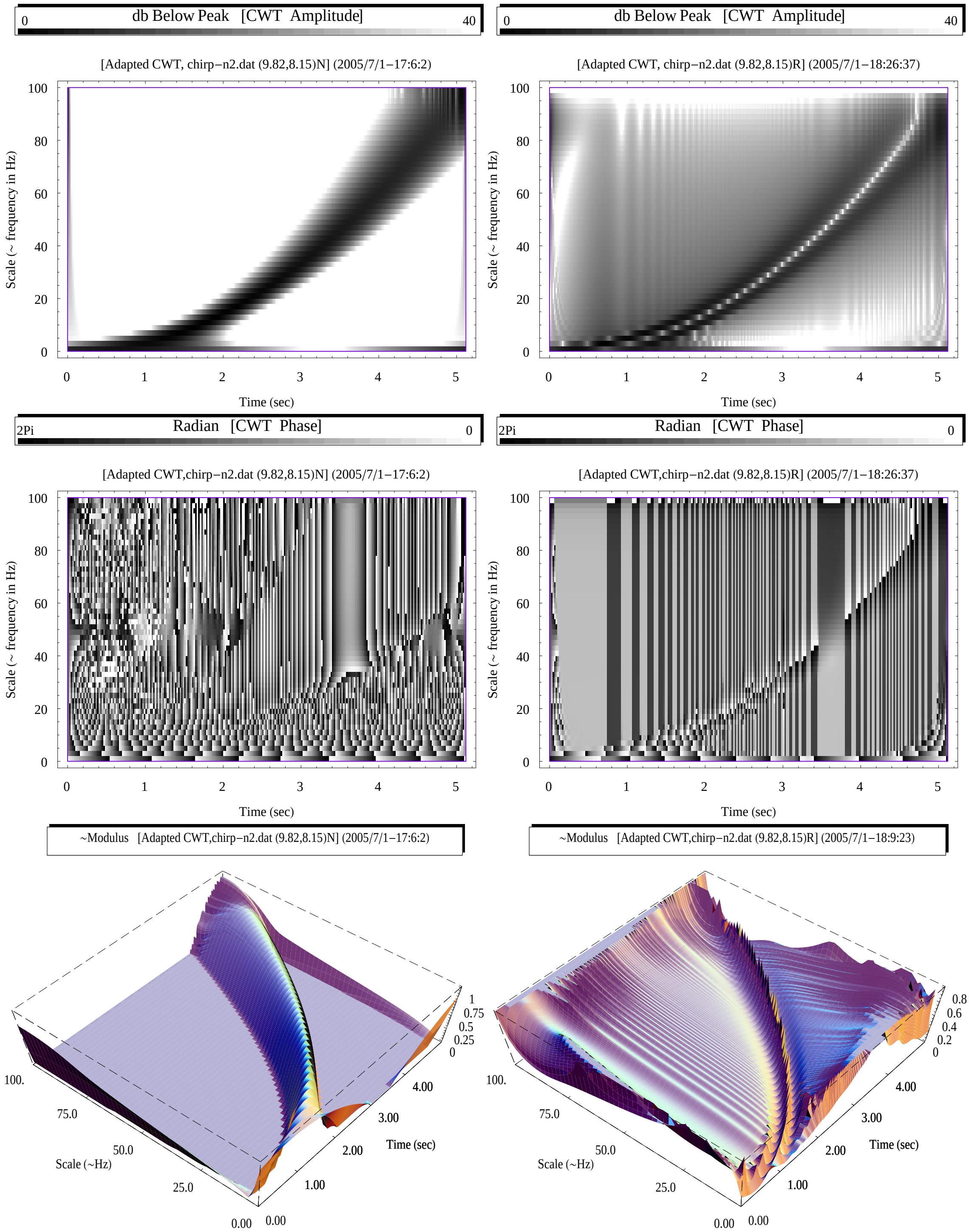

Figure 4.4: This figure shows the modulus and phase planes for the full extend of the same parabolic chirp using both the simplified Morlet wavelet (the left sub-figures) and the quasi wavelet basis function (the right sub-figures). The phase plane associated with the simplified Morlet wavelet tells little in practical significance. Note that there should be a slight up-shift correction of instantaneous frequency for the quasi wavelet basis function, and it is about $\frac{1}{0.9696}$.

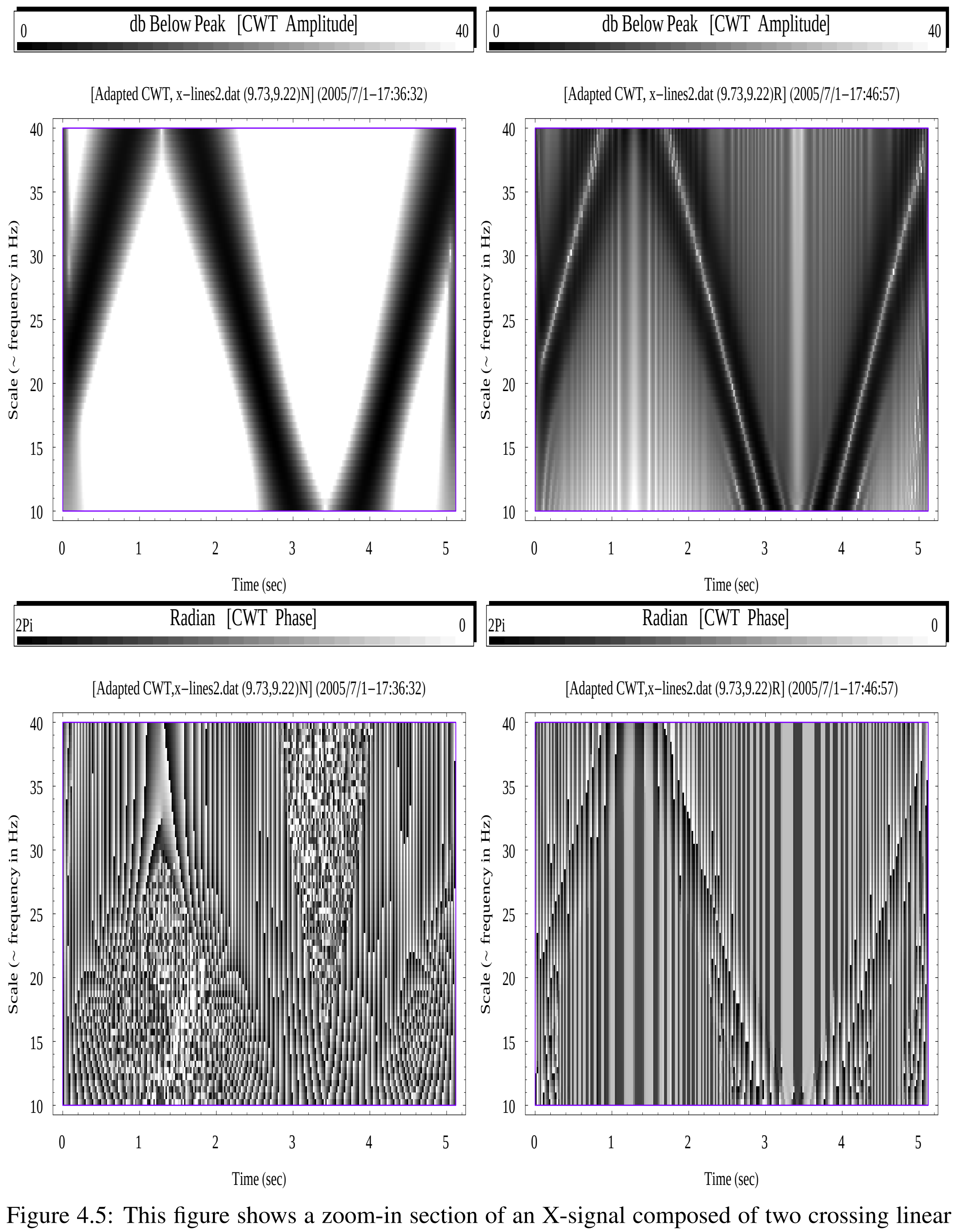

Figure 4.5: This figure shows a zoom-in section of an X-signal composed of two crossing linear chirps with equal power contents. The left sub-figures are for the simplified Morlet wavelet, and the right sub-figures are for the quasi wavelet basis function. They manifest the same depictions as given by the parabolic chirp.

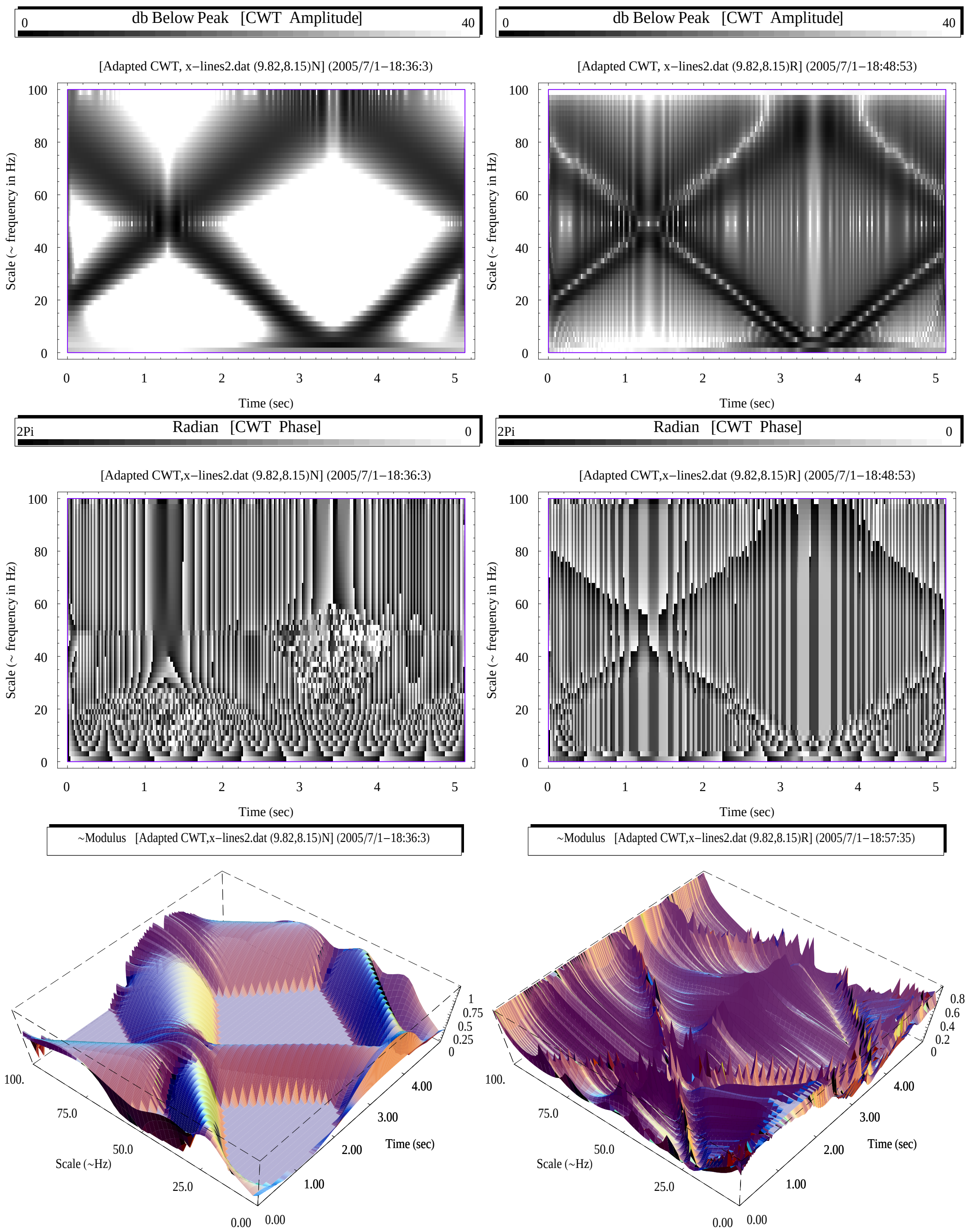

Figure 4.6: This figure shows time-frequency characterizations of the same X-signal in full extend. The left sub-figures are for the simplified Morlet wavelet and the right sub-figures are for the quasi wavelet basis function. Basically they feature identical depictions as those above, but around the intersecting region both seem to have distortions. Nevertheless, the proposed quasi wavelet basis function performs much better in phase plane rendition than does the simplified Morlet wavelet. There are saw-tooth spikes in the bottom right 3-D sub-figure, and they reflect the non-exact match between the instantaneous frequency and the numerical resolution step. The symptom can be remedied by the phase rendition (mid right sub-figure).

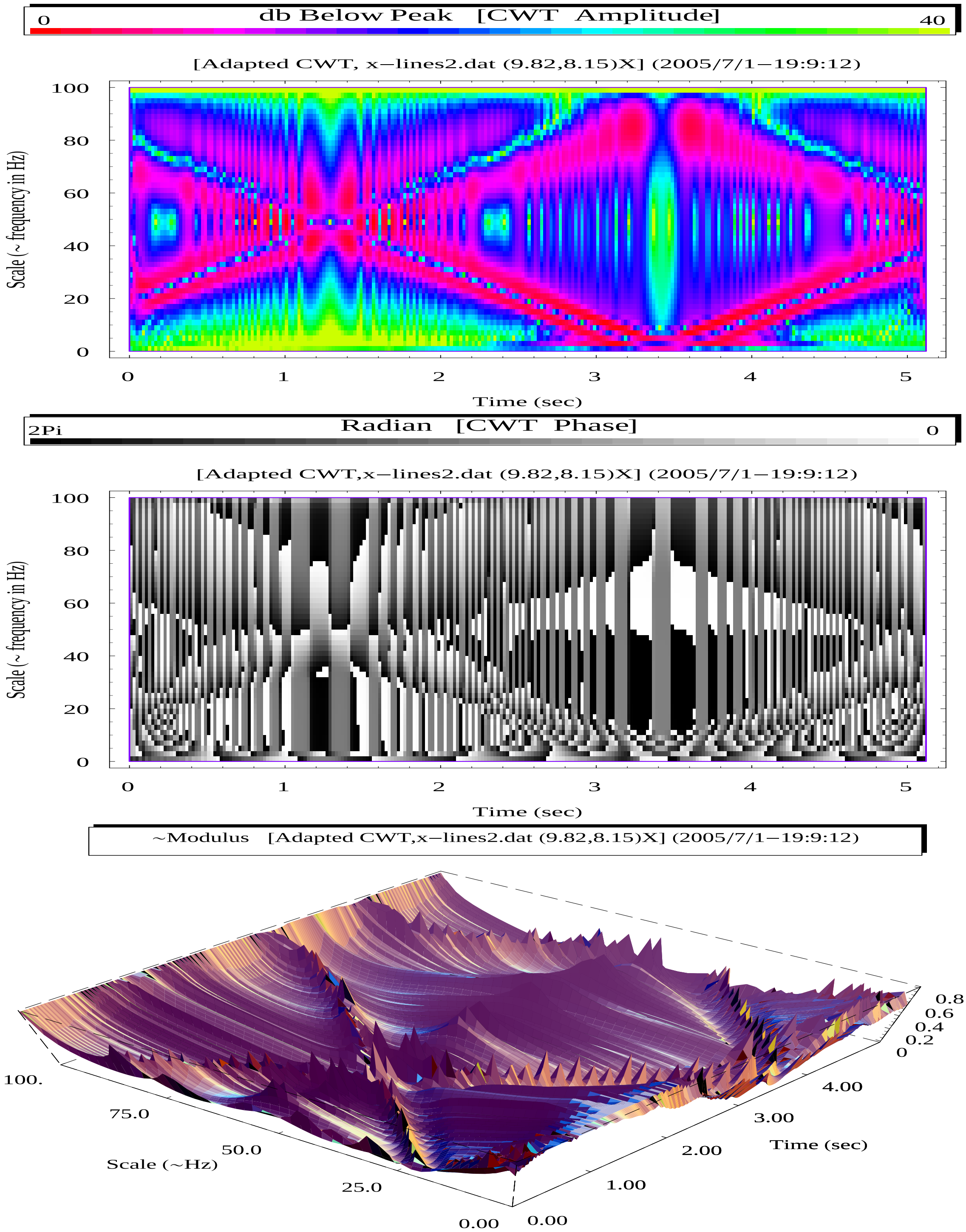

Figure 4.7: This figure illustrates the effects of phase rotation on the same X-signal based on the quasi wavelet basis function. Again, various interfacial lines in the mid sub-figure serve as indicators of the extend of frequency leakage and phase noise. It is noted that the top sub-figure is in color but may be printed in black and white.

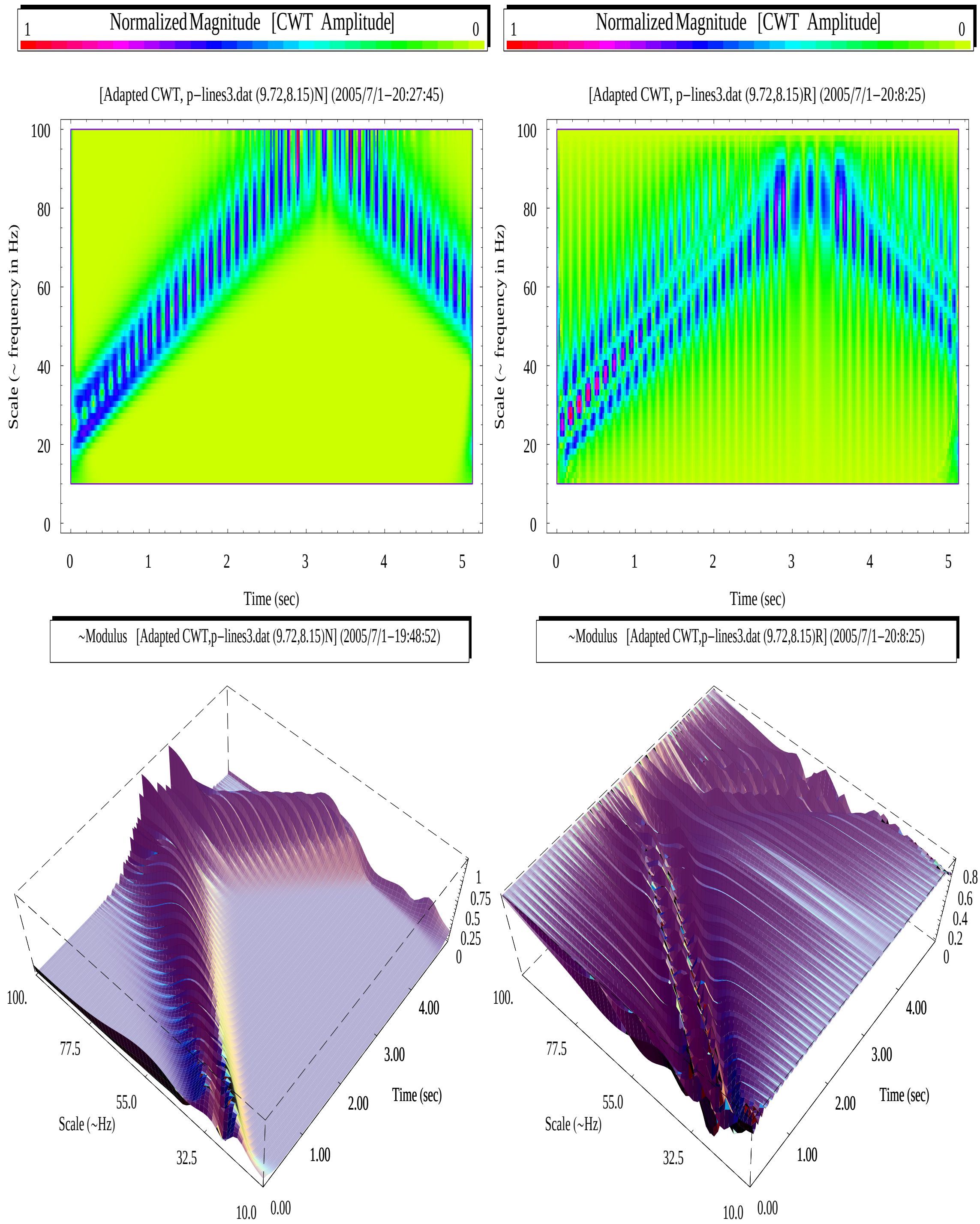

Figure 4.8: This figure shows the ridge extraction of a signal composed of a pair of parallel chirps that are with equal power contents. Here the frequency separation between the two chirps is one tenth Nyquist rate. The left sub-figures are for the simplified Morlet wavelet, and the right sub-figures are for the quasi wavelet basis function. It is clear that he power ridge given by the simplified Morlet wavelet is entirely misleading. But, for the quasi wavelet basis function, the two interfacial lines are clearly identifiable except at region near the Nyquist frequency. In the bottom right sub-figure (and several previous sub-figures), we have intentionally inverted the rendering, i.e., a trough in the 2-D plane (top right sub-figure) turns to a peak in the 3-D figure; and what are seen are the two clear spike lines.

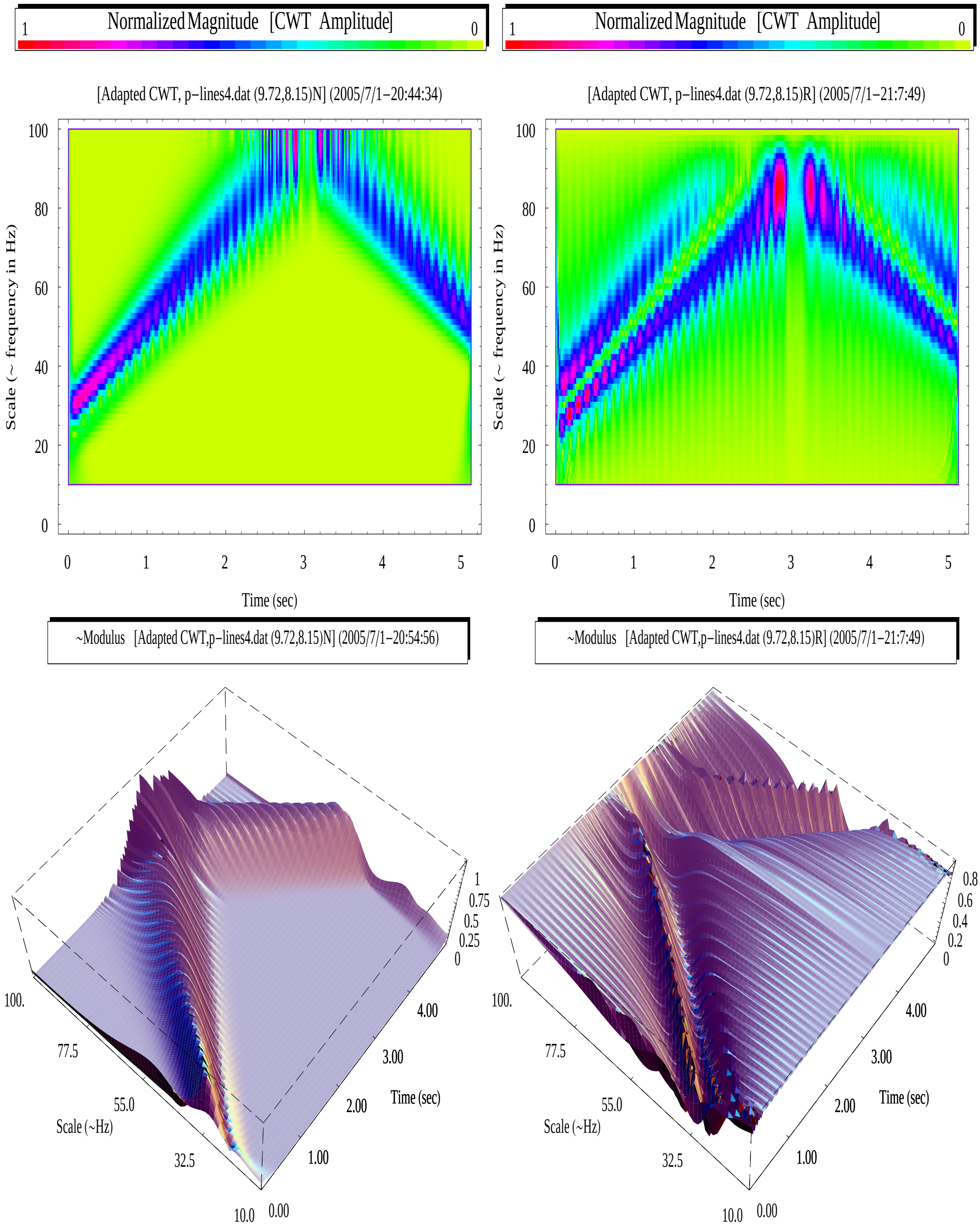

Figure 4.9: This figure shows the 2-D and 3-D modulus of a signal also composed of a pair of parallel chirps but now with energy ratio of 0.04. The left sub-figures are for the simplified Morlet wavelet, and the right sub-figures are for the quasi wavelet basis function. Both transforms show difficulty in differentiating components with power difference so large and instantaneous frequencies so proximate. There is overshadowing effects due to combined effects of frequency leakage and phase ambiguity.

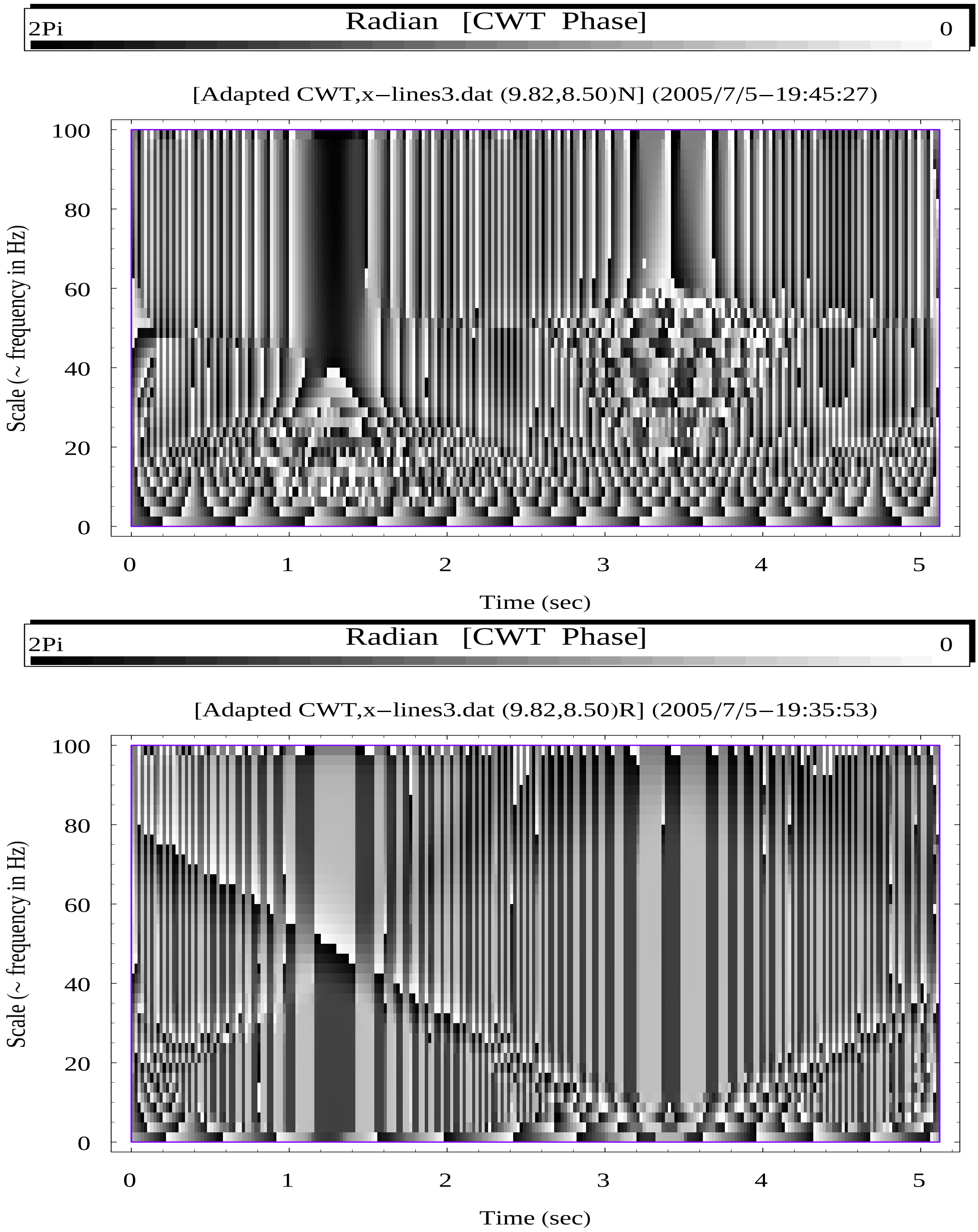

Figure 4.10: The time-frequency phase planes for an X-signal which is composed of two component chirps with power ratio of 0.01. The top and bottom sub-figures are associated with the simplified Morlet wavelet and the quasi wavelet basis function, respectively. Here, both have difficulty in rendering significant features for the weak component. But it seems that the quasi wavelet basis function is a bit more informative, especially in the low frequency region.

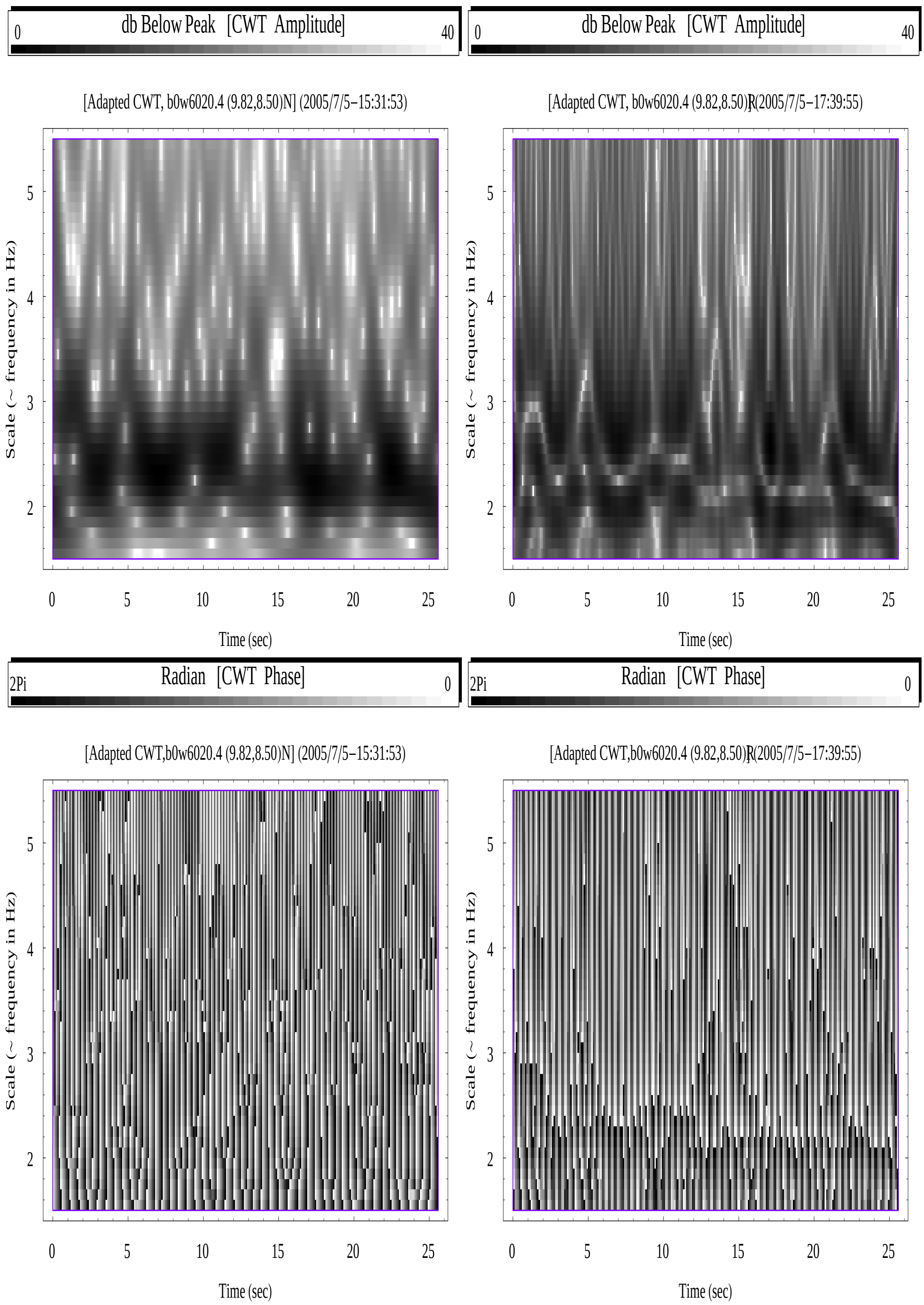

Figure 4.11: This figure show the modulus and phase renditions of a water wave signal measured in a wind blowing laboratory tank. The left sub-figures use the simplified Morlet wavelet, and right sub-figures use the proposed basis function. In general the latter ones provide easy and precise identification of the energy ridge, in particular, its phase plane rendition shows relatively outstanding features.

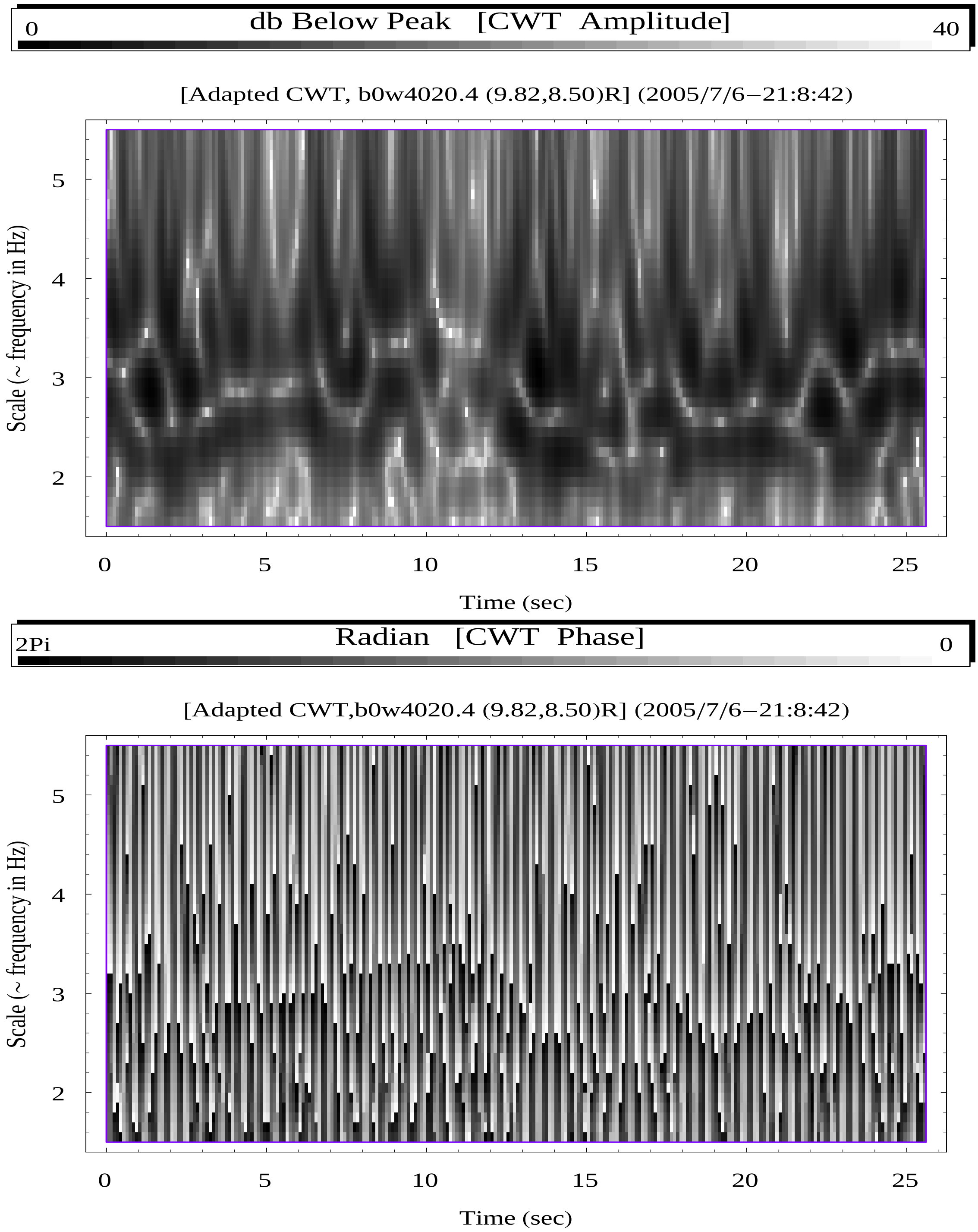

Figure 4.12: The modulus and phase planes for a lesser developed water wave signal (when compared to the previous figure, and it is due to a smaller wind speed in the tank) using the quasi wavelet basis function. The phase plane shows a very distinguish feature of multiple interfacing points along the time line. It reflects the existence of multiple scale components and the mutual interactions among them, and it also serves as the indication of instability or rapid wave modulation.

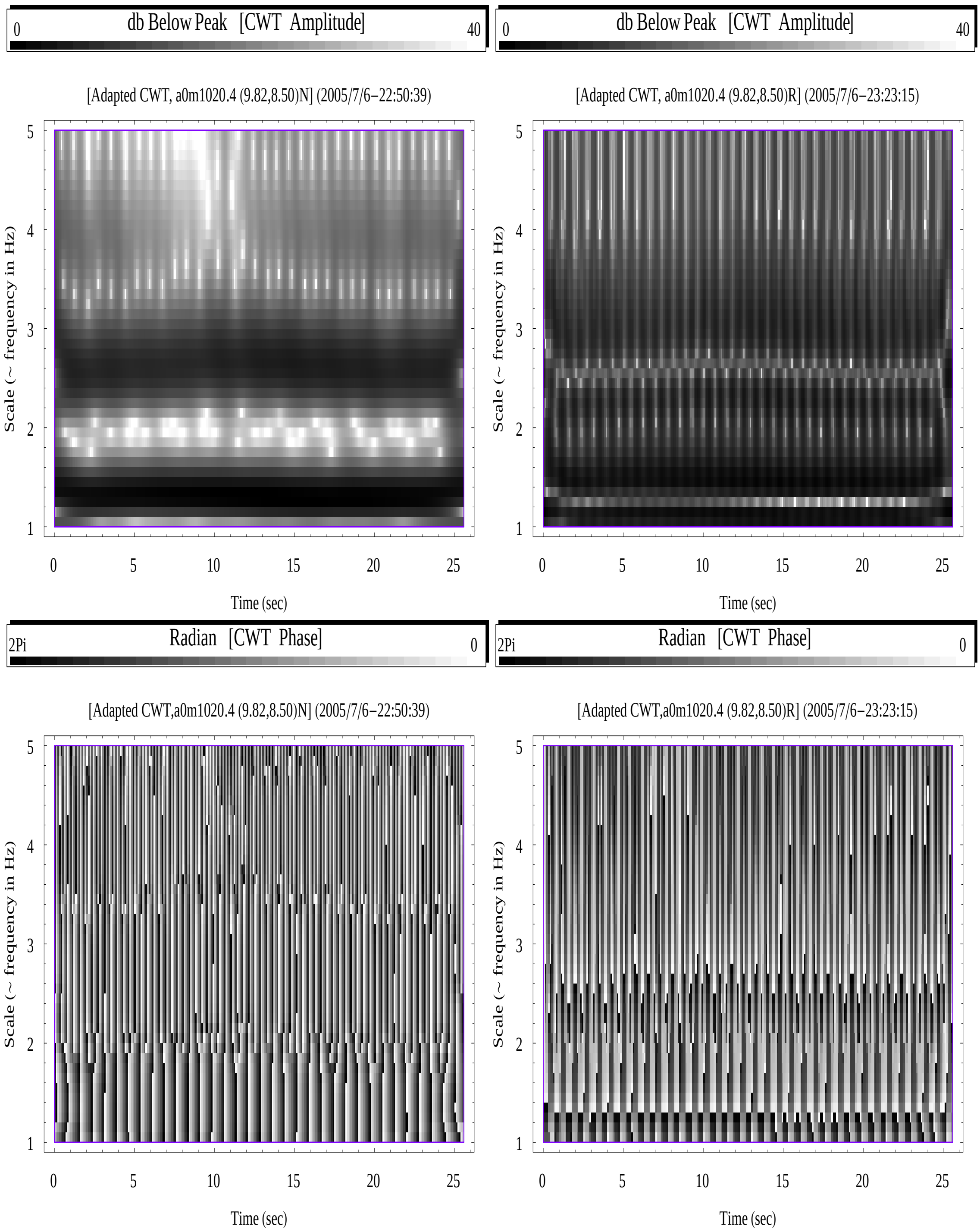

Figure 4.13: This figure compares the modulus (top sub-figures) and phase (bottom sub-figures) planes of a mechanically generated Stokes wave for both the simplified Morlet wavelet (left sub-figures) and function (right sub-figures). Here the Stokes wave has a wave steepness value of about 0.06 at its fundamental harmonic band. Again, the quasi wavelet basis shows off more interesting physics either from its modulus or phase rendition: for examples, the multi-troughs around frequency 2 to 3 Hz from both the modulus and phase renditions, the feature of rapidly oscillating (or up-and-down) interfacial points for the above troughs, and the evolution of the first fundamental harmonic. All these may serve as evidences of wave evolutions and the energy recurrence phenomenon among wave components or the Benjamin-Feir side-band instability.

Chapter 5

Conclusions

A quasi wavelet basis function is proposed, and the associated algorithm for time-frequency rendering are devised. The reasons that lead to the usefulness of the quasi wavelet basis are illustrated. Specifically, the proposed basis function's characteristic behaviors, such as the time-frequency resolutions, frequency leakages, and phase ambiguity or time smearing effects are studied, as well as respectively compared to those of the simplified Morlet wavelet.

Both numerically simulated signals and signals from wave tank experiments are used to test the functioning of the proposed quasi basis function, and these results are also compared to those of Morlet wavelet.

In general, the present quasi wavelet basis is able to provide easy and clear visual identifications of time-scale features both from the modulus and phase plane renditions. Most profoundly, the phase plane results of the proposed quasi wavelet basis are far more informative than as provided by the Morlet wavelet. In particular, they can highlight power ridge points, extends of frequency leakage, range of influence by phase noise, the oscillating ups and downs of a main component signal, and better identification of high frequency constituents.

Lastly, we note that the proposed quasi wavelet basis function lacks a few stringent requirements in mathematical or analytical robustness, such as concerning the defination of a basis, the transform completeness, the wavelet admissibility condition, and the direct calculations of modulus and phase (i.e., the present basis needs some indirect or intermediate manipulations to derive the modulus values), etc. Nonetheless, the new basis function is practically applicable and yields unique time-frequency characterizations and significant physics. ❖

BIBLIOGRAPHY

[1] Brooke Benjamin, T. Instability of periodic wave trains in nonlinear dispersive systems. *Proc. Roy. Soc. Lond.*, A299:59–75, 1967.

[2] Brooke Benjamin, T., and J. E. Feir. The disintegration of wave trains on deep water. *J. Fluid Mech.*, 27:417–430, 1967.

[3] Chui, C. K. *An Introduction to Wavelets*. Academic Press, Inc., San Diego, California, USA, 1992.

[4] Cohen, L. *Time-Frequency Analysis*. Prentice Hall PTR, Englewood Cliffs, New Jersey, USA, 1995.

[5] Daubechies, I. *Ten Lectures on Wavelets*. SIAM, Philadelphia, USA, 1992.

[6] Gabor, D. Theory of communication. *Journal of the IEE*, 93:429–457, 1946.

[7] Greenberg, M.D. *Advanced Engineering Mathematics*. Prentice Hall PTR, Englewood Cliffs, New Jersey, USA, 1988.

[8] Hwang, P. A, D. Xu, and J. Wu. Breaking of wind-generated waves: measurements and characteristics. *J. Fluid Mech.*, 202:177–200, 1989.

[9] Lake, B.M., and H.C. Yuen. A note on some nonlinear water wave experiments and comparison of data with theory. *J. Fluid Mech.*, 83:75–81, 1977.

[10] Lake, B.M., and H.C. Yuen. A new model for nonlinear gravity waves, Part 1, Physical model and experimental evidence. *J. Fluid Mech.*, 88:33–62, 1978.

[11] Lake, B.M., H.C. Yuen, H. Rundgaldier, and W.E. Ferguson. Nonlinear deep-water waves: Theory and experiment, Part 2, Evolution of a continuous wave train. *J. Fluid Mech.*, 83:49–74, 1977.

[12] Lee, Y.R. Signal analysis from wave modulation perspective – Part I: Characterizing the analytic signal procedure. Technical report, No.1997–7, Institute of Harbor and Marine Technology, Taichung, Taiwan, 1997.

[13] Lee, Y.R. The search of the most appropriate function basis for laboratory water waves. Technical report, No.1998–5(II), Institute of Harbor and Marine Technology, Taichung, Taiwan, 1998.

[14] Lee, Y.R. Wave Characterizations Using Wavelet and Spectral Coherences. Technical report, No.2001–08, Institute of Harbor and Marine Technology, Taichung, Taiwan, 2000.

[15] Lee, Y.R. Signal Analysis from Wave Modulation Perspective. Technical report, No.2001–09, Institute of Harbor and Marine Technology, Taichung, Taiwan, 2001.

[16] Lee, Y.R. Wavelet Time-Frequency Analysis - An Optimum Basis and Its Applications to Water Waves. Technical report, No.93-79-7112, Institute of Harbor and Marine Technology, Taichung, Taiwan, 2003.

[17] Lee, Y.R., and J. Wu. Continuous wavelet transform using a locally adapted time-frequency window. In *Proc. 18th Conf. On Ocean Engineering in Taiwan*, pages 95–106, 1996.

[18] Lee, Y.R., and J. Wu. Wavelet and wavelet packet best basis for laboratory water waves. In *Proc. 18th Conf. On Ocean Engineering in Taiwan*, pages 83–94, 1996.

[19] Lee, Y.R., and J. Wu. Time-frequency features and side band instability. In *Proc. 19th Conf. On Ocean Engineering in Taiwan*, pages 32–39, 1997.

[20] Lee, Y.R., and J. Wu. Wavelet coherences based on an optimum analyzing function basis. In *Proc. 20th Conf. On Ocean Engineering in Taiwan*, pages 109–116, 1998.

[21] Lee, Y.R., and J. Wu. The wavelet optimum basis and the phase distribution of the characteristic function. *Proc. 25th Conf. on Ocean Engineering in Taiwan*, pages 149–156, 2003.

[22] Longuet-Higgins, M.S. The instability of gravity waves of finite amplitude in deep water I, Superharmonics. *Proc. Roy. Soc. Lond.*, A360:471–488, 1978.

[23] Longuet-Higgins, M.S. The instability of gravity waves of finite amplitude in deep water II, Subharmonics. *Proc. Roy. Soc. Lond.*, A360:489–505, 1978.

[24] M. B. Ruskai, G. Beylkin, R. Coifman, I. Daubechies, S. Mallat, Y. Meyer, and L. Raphael, editor. *Wavelets and Their Applications*. Jones and Bartlett Publishers, Boston, New York, USA, 1992.

[25] Mallat, S. *A Wavelet Tour of Signal Processing*. Academic Press, Inc., San Diego, California, USA, 1998.

[26] Mallat, S., and S. Zhong. Wavelet transform maxima and multiscale edges. In M. B. Ruskai, G. Beylkin, R. Coifman, I. Daubechies, S. Mallat, Y. Meyer, and L. Raphael, editor, *Wavelets and Their Applications*, pages 67–104. Jones and Bartlett Publishers, Boston, New York, USA, 1992.

[27] Melville, W. K. The instability and breaking of deep water waves. *J. Fluid Mech.*, 115:165–185, 1982.

[28] Melville, W. K. Wave modulation and breakdown. *J. Fluid Mech.*, 128:489–506, 1983.

[29] Meyer, Y. *Wavelets and operators*. Cambridge University Press, New York, USA, 1992.

[30] Su, M.Y. Evolution of groups of gravity waves with moderate to high steepness. *Phys. Fluids*, 25:2167–2174, 1982.

[31] Tchamitchian, Ph., and B. Torresani. Ridge and skeleton extraction from the wavelet transform. In M. B. Ruskai, G. Beylkin, R. Coifman, I. Daubechies, S. Mallat, Y. Meyer, and L. Raphael, editor, *Wavelets and Their Applications*, pages 123–151. Jones and Bartlett Publishers, Boston, New York, USA, 1992.

[32] Yuen, H. C., and B. M. Lake. Nonlinear deep water waves: Theory and experiment. *Phys. Fluids*, 18:956–960, 1975.

BIBLIOGRAPHY

[1] Brooke Benjamin, T. Instability of periodic wave trains in nonlinear dispersive systems. *Proc. Roy. Soc. Lond.*, A299:59–75, 1967.

[2] Brooke Benjamin, T., and J. E. Feir. The disintegration of wave trains on deep water. *J. Fluid Mech.*, 27:417–430, 1967.

[3] Chui, C. K. *An Introduction to Wavelets*. Academic Press, Inc., San Diego, California, USA, 1992.

[4] Cohen, L. *Time-Frequency Analysis*. Prentice Hall PTR, Englewood Cliffs, New Jersey, USA, 1995.

[5] Daubechies, I. *Ten Lectures on Wavelets*. SIAM, Philadelphia, USA, 1992.

[6] Gabor, D. Theory of communication. *Journal of the IEE*, 93:429–457, 1946.

[7] Greenberg, M.D. *Advanced Engineering Mathematics*. Prentice Hall PTR, Englewood Cliffs, New Jersey, USA, 1988.

[8] Hwang, P. A, D. Xu, and J. Wu. Breaking of wind-generated waves: measurements and characteristics. *J. Fluid Mech.*, 202:177–200, 1989.

[9] Lake, B.M., and H.C. Yuen. A note on some nonlinear water wave experiments and comparison of data with theory. *J. Fluid Mech.*, 83:75–81, 1977.

[10] Lake, B.M., and H.C. Yuen. A new model for nonlinear gravity waves, Part 1, Physical model and experimental evidence. *J. Fluid Mech.*, 88:33–62, 1978.

[11] Lake, B.M., H.C. Yuen, H. Rundgaldier, and W.E. Ferguson. Nonlinear deep-water waves: Theory and experiment, Part 2, Evolution of a continuous wave train. *J. Fluid Mech.*, 83:49–74, 1977.

[12] Lee, Y.R. Signal analysis from wave modulation perspective – Part I: Characterizing the analytic signal procedure. Technical report, No.1997–7, Institute of Harbor and Marine Technology, Taichung, Taiwan, 1997.

[13] Lee, Y.R. The search of the most appropriate function basis for laboratory water waves. Technical report, No.1998–5(II), Institute of Harbor and Marine Technology, Taichung, Taiwan, 1998.

[14] Lee, Y.R. Wave Characterizations Using Wavelet and Spectral Coherences. Technical report, No.2001–08, Institute of Harbor and Marine Technology, Taichung, Taiwan, 2000.

[15] Lee, Y.R. Signal Analysis from Wave Modulation Perspective. Technical report, No.2001–09, Institute of Harbor and Marine Technology, Taichung, Taiwan, 2001.

[16] Lee, Y.R. Wavelet Time-Frequency Analysis - An Optimum Basis and Its Applications to Water Waves. Technical report, No.93-79-7112, Institute of Harbor and Marine Technology, Taichung, Taiwan, 2003.

[17] Lee, Y.R., and J. Wu. Continuous wavelet transform using a locally adapted time-frequency window. In *Proc. 18th Conf. On Ocean Engineering in Taiwan*, pages 95–106, 1996.

[18] Lee, Y.R., and J. Wu. Wavelet and wavelet packet best basis for laboratory water waves. In *Proc. 18th Conf. On Ocean Engineering in Taiwan*, pages 83–94, 1996.

[19] Lee, Y.R., and J. Wu. Time-frequency features and side band instability. In *Proc. 19th Conf. On Ocean Engineering in Taiwan*, pages 32–39, 1997.

[20] Lee, Y.R., and J. Wu. Wavelet coherences based on an optimum analyzing function basis. In *Proc. 20th Conf. On Ocean Engineering in Taiwan*, pages 109–116, 1998.

[21] Lee, Y.R., and J. Wu. The wavelet optimum basis and the phase distribution of the characteristic function. *Proc. 25th Conf. on Ocean Engineering in Taiwan*, pages 149–156, 2003.

[22] Longuet-Higgins, M.S. The instability of gravity waves of finite amplitude in deep water I, Superharmonics. *Proc. Roy. Soc. Lond.*, A360:471–488, 1978.

[23] Longuet-Higgins, M.S. The instability of gravity waves of finite amplitude in deep water II, Subharmonics. *Proc. Roy. Soc. Lond.*, A360:489–505, 1978.

定價 元

新型類仔波函數及其時尺轉換特性與應用

交通部運輸研究所

GPN:1009301566
定價 元

[24] M. B. Ruskai, G. Beylkin, R. Coifman, I. Daubechies, S. Mallat, Y. Meyer, and L. Raphael, editor. *Wavelets and Their Applications*. Jones and Bartlett Publishers, Boston, New York, USA, 1992.

[25] Mallat, S. *A Wavelet Tour of Signal Processing*. Academic Press, Inc., San Diego, California, USA, 1998.

[26] Mallat, S., and S. Zhong. Wavelet transform maxima and multiscale edges. In M. B. Ruskai, G. Beylkin, R. Coifman, I. Daubechies, S. Mallat, Y. Meyer, and L. Raphael, editor, *Wavelets and Their Applications*, pages 67–104. Jones and Bartlett Publishers, Boston, New York, USA, 1992.

[27] Melville, W. K. The instability and breaking of deep water waves. *J. Fluid Mech.*, 115:165–185, 1982.

[28] Melville, W. K. Wave modulation and breakdown. *J. Fluid Mech.*, 128:489–506, 1983.

[29] Meyer, Y. *Wavelets and operators*. Cambridge University Press, New York, USA, 1992.

[30] Su, M.Y. Evolution of groups of gravity waves with moderate to high steepness. *Phys. Fluids*, 25:2167–2174, 1982.

[31] Tchamitchian, Ph., and B. Torresani. Ridge and skeleton extraction from the wavelet transform. In M. B. Ruskai, G. Beylkin, R. Coifman, I. Daubechies, S. Mallat, Y. Meyer, and L. Raphael, editor, *Wavelets and Their Applications*, pages 123–151. Jones and Bartlett Publishers, Boston, New York, USA, 1992.

[32] Yuen, H. C., and B. M. Lake. Nonlinear deep water waves: Theory and experiment. *Phys. Fluids*, 18:956–960, 1975.